JACS
JOURNAL OF THE AMERICAN CHEMICAL SOCIETY
Article
pubs.acs.org/JACS

Olefin Isomerization by Iridium Pincer Catalysts. Experimental Evidence for an η^3-Allyl Pathway and an Unconventional Mechanism Predicted by DFT Calculations

Soumik Biswas,[†] Zheng Huang,[‡] Yuriy Choliy,[†] David Y. Wang,[†] Maurice Brookhart,*[,‡] Karsten Krogh-Jespersen,*[,†] and Alan S. Goldman*[,†]

[†]Department of Chemistry and Chemical Biology, Rutgers, The State University of New Jersey, New Brunswick, New Jersey 08903, United States

[‡]Department of Chemistry, The University of North Carolina at Chapel Hill, Chapel Hill, North Carolina 27599, United States

Supporting Information

ABSTRACT: The isomerization of olefins by complexes of the pincer-ligated iridium species ($^{t\mathrm{Bu}}$PCP)Ir ($^{t\mathrm{Bu}}$PCP = κ^3-C_6H_3-2,6-$(CH_2P^tBu_2)_2$) and ($^{t\mathrm{Bu}}$POCOP)Ir ($^{t\mathrm{Bu}}$POCOP = κ^3-C_6H_3-2,6-$(OP^tBu_2)_2$) has been investigated by computational and experimental methods. The corresponding dihydrides, (pincer)IrH_2, are known to hydrogenate olefins via initial Ir−H addition across the double bond. Such an addition is also the initial step in the mechanism most widely proposed for olefin isomerization (the "hydride addition pathway"); however, the results of kinetics experiments and DFT calculations (using both M06 and PBE functionals) indicate that this is not the operative pathway for isomerization in this case. Instead, (pincer)Ir(η^2-olefin) species undergo isomerization via the formation of (pincer)Ir(η^3-allyl)(H) intermediates; one example of such a species, ($^{t\mathrm{Bu}}$POCOP)Ir(η^3-propenyl)(H), was independently generated, spectroscopically characterized, and observed to convert to ($^{t\mathrm{Bu}}$POCOP)Ir(η^2-propene). Surprisingly, the DFT calculations indicate that the conversion of the η^2-olefin complex to the η^3-allyl hydride takes place via initial dissociation of the Ir−olefin π-bond to give a σ-complex of the allylic C−H bond; this intermediate then undergoes C−H bond oxidative cleavage to give an iridium η^1-allyl hydride which "closes" to give the η^3-allyl hydride. Subsequently, the η^3-allyl group "opens" in the opposite sense to give a new η^1-allyl (thus completing what is formally a 1,3 shift of Ir), which undergoes C−H elimination and π-coordination to give a coordinated olefin that has undergone double-bond migration.

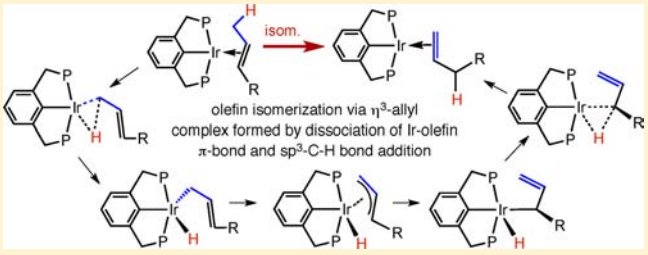

INTRODUCTION

Examples of transition-metal-catalyzed olefin isomerization are widespread and play a key role in numerous important chemical processes.[1−9] The mechanism most commonly accepted for olefin isomerization involves initial addition of a metal−H bond across the olefin double bond. If the resulting metal alkyl has a β-carbon atom that is inequivalent to the carbon to which the hydride was added, β-elimination of hydrogen from that carbon will result in olefin isomerization (Scheme 1a). An alternative pathway, less commonly proposed and less well-studied, involves the intermediacy of a π-allyl complex (Scheme 1b) through which olefin isomerization occurs via a formal 1,3-hydride shift.[1,2,10−14] If a coordinatively unsaturated metal complex bears a metal-bound hydride, the hydride addition pathway is believed to be the preferred mechanism for olefin isomerization.[1]

We have recently reported a tandem catalytic system for the metathesis of alkanes, comprising an iridium pincer catalyst for alkane dehydrogenation/olefin hydrogenation and a second catalyst for olefin metathesis (Scheme 2).[15,16] Alkane metathesis[17,18] (AM) can potentially be employed for the transformation of low molecular weight alkanes into higher molecular weight alkanes; this will likely become increasingly important as conventional

Scheme 1. Schematic Illustration of the Two Mechanism Classes Proposed for Olefin Isomerization: (a) "Hydride" Mechanism, (b) π-Allyl Mechanism

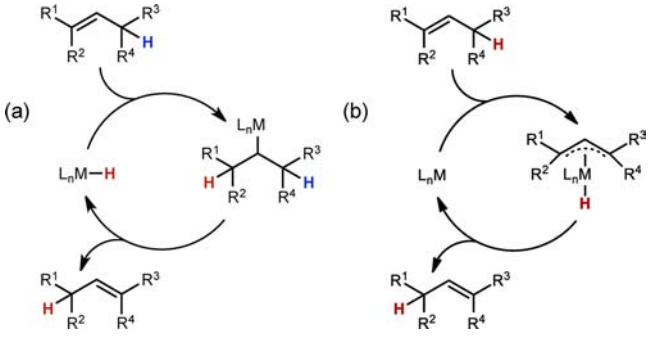

Received: February 13, 2012
Published: July 5, 2012

dx.doi.org/10.1021/ja301464c | J. Am. Chem. Soc. 2012, 134, 13276−13295

Scheme 2. Tandem Catalytic Alkane Metathesis with Pincer-Ligated Iridium Complexes and Olefin Metathesis Catalysts (Shown for Reaction of *n*-Hexane)

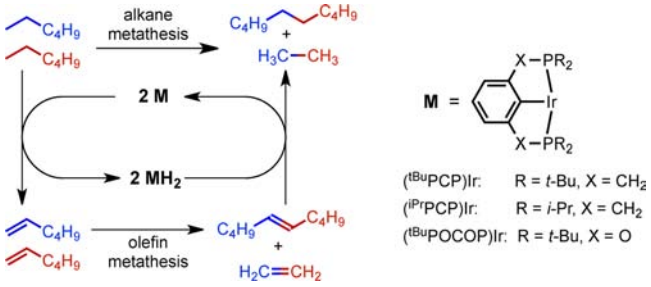

petroleum reserves dwindle. For example, Fischer–Tropsch product mixtures (primarily *n*-alkanes)[19] as well as natural gas condensates[20] include C_3–C_8 *n*-alkane fractions that are not directly suitable for most transportation fuels. Conversion to the corresponding C_{2n-2} species, such as conversion of *n*-hexane to *n*-decane plus ethane, could give access to heavier (C_{9-19}) *n*-alkanes, which constitute a valuable clean-burning diesel fuel. Previously reported AM systems, however, have not shown such desirable selectivity for the formation of C_{2n-2} species from C_n substrates.[17,18]

The AM systems developed in our laboratories are mainly based on two types of pincer catalysts, (^{R}PCP)Ir (^{R}PCP = κ^3-C_6H_3-2,6-$(CH_2PR_2)_2$) and (^{R}POCOP)Ir (^{R}POCOP = κ^3-C_6H_3-2,6-$(OPR_2)_2$), employed in combination with a Schrock-type olefin metathesis catalyst.[21] Iridium pincer catalysts, including ($^{t\mathrm{Bu}}$PCP)Ir and ($^{i\mathrm{Pr}}$PCP)Ir, have been found to dehydrogenate *n*-alkanes with kinetic selectivity to form α-olefins.[22] Thus, these systems might be expected to selectively produce ethane and C_{2n-2} species, as shown in the example in Scheme 2 (metathesis of *n*-hexane to yield ethane and *n*-decane); in fact, AM of *n*-hexane generates a range of C_2 to C_{15} *n*-alkanes.[15,16] Significantly, the ($^{t\mathrm{Bu}}$PCP)Ir system gives moderate selectivity for the formation of *n*-decane (ca. 50 mol % of the C_n products where $n > 6$), whereas the ($^{t\mathrm{Bu}}$POCOP)Ir system gives an essentially stochastic distribution of *n*-alkanes.[15,16] The most obvious explanation for the initial formation of C_{3-5} and C_{7-9} products from *n*-hexane is based upon isomerization/metathesis of the olefin intermediates prior to hydrogenation. A significant degree of isomerization of 1-alkenes has indeed been previously reported when pincer–Ir complexes are used for either acceptorless or transfer dehydrogenation of *n*-alkanes.[23] In consideration of these issues, we initiated a study of pincer–iridium-catalyzed olefin isomerization with an emphasis on comparison between the ($^{t\mathrm{Bu}}$PCP)Ir and ($^{t\mathrm{Bu}}$POCOP)Ir systems.

With either PCP or POCOP ligands, five-coordinate (pincer)IrH_2 species are intermediates in alkane dehydrogenation.[22,24,25] The insertion of C–C double bonds into the Ir–H bonds of these complexes is a necessary step in the overall cycle for alkane metathesis and for transfer dehydrogenation more generally. Thus, catalytic olefin isomerization by the pincer–iridium complexes was initially assumed to proceed via the insertion mechanism (i.e., Ir–H addition) illustrated in Scheme 3. A 2,1 insertion of 1-alkene into the Ir–H bond of the (pincer)IrH_2 complex, followed by β-H elimination from the *n*-alkyl group, would generate the isomeric 2-olefin product.[22] Surprisingly, however, experimental and computational evidence supports a π-allyl pathway for both complexes (Scheme 1b). Even more surprisingly, although π-allyl pathways are well-established, our results strongly indicate that the stepwise

Scheme 3. Possible Olefin Insertion Pathway (Hydride Pathway) for Isomerization by Pincer–Iridium Complexes

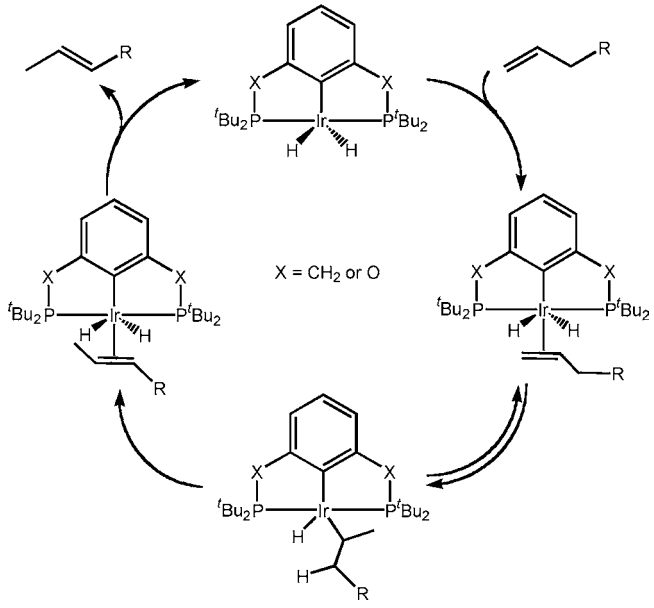

mechanism is quite different from that which is conventionally proposed for π-allyl pathways. This conclusion has implications for catalytic AM, for alkane dehydrogenation systems more generally, and, potentially, for any system involving transition-metal-catalyzed olefin isomerization or the formation of an η^3-allyl complex from an olefin.

RESULTS AND DISCUSSION

AM Catalyst Resting State. Typical AM reactions are performed at 125 °C in *n*-alkane as solvent and reactant, with 10 mM of pincer–iridium dehydrogenation catalyst and ca. 16 mM Mo(*N*-2,6-(*i*-Pr)$_2$C$_6$H$_3$)(CHCMe$_2$Ph)[OC-$(CF_3)_2(CH_3)]_2$[21] ("Mo-F12") olefin metathesis catalyst in *n*-alkane as solvent and reactant. When an iridium dihydride is used as the catalyst, 2 equiv of *t*-butylethylene per mol iridium dihydride is typically added; 1 equiv serves to dehydrogenate the catalyst, while the second equivalent acts as an acceptor for hydrogen from *n*-alkane and thereby serves to establish a steady-state concentration of 1 equiv olefin per mol catalyst. No *t*-butylethylene is added when ($^{t\mathrm{Bu}}$POCOP)Ir(C_2H_4) is used as precursor since this precatalyst does not need to be dehydrogenated and the mol of C_2H_4 acts as an acceptor to establish the steady-state concentration of olefin.

Our investigation of the mechanistic aspects of AM, including the olefin isomerization component, began with in situ observations of the catalyst resting state. ^{31}P NMR spectroscopy reveals that, under the typical conditions noted above, the resting state for the ($^{t\mathrm{Bu}}$PCP)Ir system is ($^{t\mathrm{Bu}}$PCP)IrH_2 (**1**); no other species are observed in the ^{31}P NMR spectrum.[14] In contrast, for the ($^{t\mathrm{Bu}}$POCOP)Ir system, only ($^{t\mathrm{Bu}}$POCOP)Ir(olefin) species are observed to be present by ^{31}P NMR spectroscopy.[14] Thus, if it were assumed that olefin isomerization proceeds via the hydride insertion mechanism, it might be expected that the ($^{t\mathrm{Bu}}$POCOP)Ir system would be *less* active with respect to isomerization and might therefore impart *higher* selectivity in AM, in sharp contrast to the observed results. This apparent anomaly initially led us to probe the mechanism of olefin isomerization by each of these pincer systems.

dx.doi.org/10.1021/ja301464c | J. Am. Chem. Soc. 2012, 134, 13276–13295

Kinetics of Catalytic Isomerization. Effect of Alkane versus Arene Solvent: Evidence against a Hydride Mechanism. A kinetic study of the isomerization of 1-octene catalyzed by ($^{t\text{Bu}}$PCP)IrH$_2$ (**1**) was conducted using *n*-octane or *p*-xylene as solvents (eq 1). Addition of 1-octene (100 mM) to **1** (5 mM), in either solvent, results in apparently quantitative conversion to ($^{t\text{Bu}}$PCP)Ir(1-octene) within 10 min at 25 °C (eq 2). However, as indicated by the equilibrium of eq 2, the

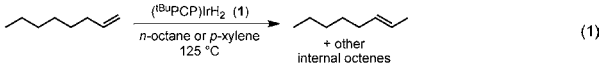

(1)

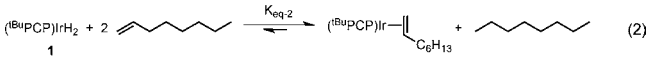

(2)

$$[\mathbf{1}] = (1/K_{eq\text{-}2}) \cdot [n\text{-octane}] \cdot [(^{t\text{Bu}}\text{PCP})\text{Ir(1-octene)}] / [\text{1-octene}]^2$$

concentration of dihydride complex **1**, although minor, would presumably be much greater in *n*-octane than in *p*-xylene. (The equilibrium expression for the concentration of **1** is not rigorous because it neglects all sources of hydrogen other than *n*-octane, but certainly any steady-state concentration of **1** would be much greater in alkane solvent than in *p*-xylene, which cannot easily act as a hydrogen donor.) Therefore, if a minor concentration of **1** were actually the major active olefin isomerization catalyst, olefin isomerization would be much faster in the alkane solvent. In fact, the rates of isomerization are equal (within 1%) in *n*-octane and *p*-xylene solvent (Figure 1). These results argue strongly against operation of the hydride addition mechanism for ($^{t\text{Bu}}$PCP)Ir-catalyzed olefin isomerization.

The turnover frequency (k) for eq 1 in either solvent is 4.2×10^{-3} s^{-1} at 125 °C (rate = k[($^{t\text{Bu}}$PCP)Ir]; $\Delta G^{\ddagger} \sim$ 27.9 kcal/mol). A zero-order dependence on [1-octene] is observed (Figure 1), which is consistent with an intramolecular π-allyl mechanism in which ($^{t\text{Bu}}$PCP)Ir(1-octene) is the major resting state (as is observed by NMR spectroscopy), and the rate-determining step lies within segments (a), (b), or (c) of the cycle indicated in Scheme 4. (We define these as "segments" of the cycle since each of them, and particularly (a) or (b), could involve more than one elementary reaction step.)

Consistent with the mechanism of Scheme 4, loss of alkene from ($^{t\text{Bu}}$PCP)Ir(alkene) is rapid and dissociative. Exchange spectroscopy (EXSY) experiments reveal that at 25 °C the rate of 1-hexene dissociation is 0.51 s^{-1} and independent of the concentration of added 1-hexene. An Eyring plot based on rates measured at temperatures between 20 and 46 °C affords activation parameters $\Delta H^{\ddagger}$ = 21.4 ± 0.8 kcal/mol and $\Delta S^{\ddagger}$ = 12 ± 3 eu for loss of 1-hexene. Dissociation of *trans*-2-hexene, as would be expected of a dissociative process with a bulkier ligand, is even faster; at 4 °C, the rate is 3.1 s^{-1}, independent of

Scheme 4. Schematic π-Allyl Pathway for 1-Alkene Isomerization with Dissociative Olefin Exchange (Detailed Mechanism Not Specified)

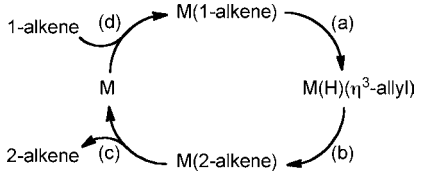

the concentration of added *trans*-2-hexene, with activation parameters determined to be $\Delta H^{\ddagger}$ = 15.4 ± 0.4 kcal/mol and $\Delta S^{\ddagger}$ = −0.7 ± 1.5 eu (from rates measured at temperatures ranging from −17 to 6 °C). Extrapolation to 125 °C yields a value (2×10^4 s^{-1}) that is orders of magnitude greater than the overall rate of isomerization.

These kinetic experiments were repeated with ($^{t\text{Bu}}$POCOP)-IrH$_2$ (**2**) as the catalyst precursor. As was the case with ($^{t\text{Bu}}$PCP)IrH$_2$, ($^{t\text{Bu}}$POCOP)Ir(1-octene) was formed rapidly and apparently quantitatively and remained the major species in solution during the catalysis, as determined by in situ ^{31}P NMR spectroscopy. No significant difference in isomerization rates was found using *n*-octane as solvent versus *p*-xylene (Figure 2);

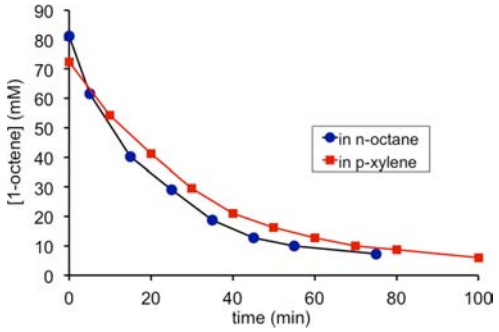

Figure 2. Isomerization of 1-octene to internal octenes catalyzed by ($^{t\text{Bu}}$POCOP)IrH$_2$ at 125 °C: (a) *n*-octane solvent, (b) *p*-xylene solvent.

again, this argues strongly against operation of the hydride addition mechanism.

In contrast with the ($^{t\text{Bu}}$PCP)Ir-catalyzed reaction, however, in the case of ($^{t\text{Bu}}$POCOP)Ir, the reaction kinetics show a clear positive dependence on 1-octene concentration. Given that the 1-octene complex is observed to be the major species in solution, this is not easily reconciled with a hydride insertion mechanism since the steady-state concentration of ($^{t\text{Bu}}$POCOP)IrH$_2$ should be *inverse-second-order* in [1-octene]

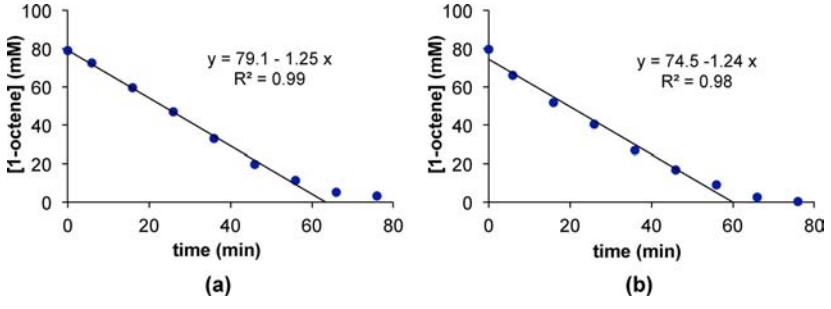

Figure 1. Catalytic isomerization of 1-octene to internal octenes by **1** (5 mM) at 125 °C: (a) *n*-octane solvent, (b) *p*-xylene solvent.

dx.doi.org/10.1021/ja301464c | J. Am. Chem. Soc. 2012, 134, 13276−13295

(and first-order in *n*-octane) (cf. eq 2). This positive dependence on [1-octene] is, however, also inconsistent with a π-allyl mechanism operating with ($^{t\mathrm{Bu}}$POCOP)Ir(1-octene) as the resting state, unless the rate-determining step involves an additional equivalent of 1-octene. While this would be the case if loss of 2-alkene (step c in Scheme 4) were reversible and the back-reaction with 2-octene were fast relative to addition of 1-alkene, these conditions seem highly unlikely given the lesser bulkiness and initially higher concentration of 1-alkenes.

An alternative explanation for the positive dependence of rate on [1-alkene] is that formation of ($^{t\mathrm{Bu}}$POCOP)Ir(2-alkene) is reversible, and that displacement of coordinated 2-alkene by 1-alkene proceeds through an *associative* rate-determining step; such a pathway is indicated in Scheme 5. Activation enthalpies

Scheme 5. Alternative π-Allyl Pathway for 1-Alkene Isomerization, Involving Associative Displacement of 2-Alkene by 1-Alkene

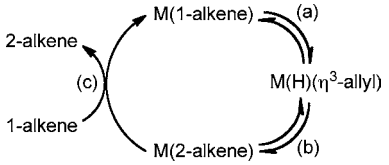

for self-exchange for ($^{t\mathrm{Bu}}$POCOP)Ir(olefin) were determined by EXSY spectroscopy to be 29.4 ± 1.2 and 26.0 ± 1.2 kcal/mol for 1-hexene and *trans*-2-hexene, respectively, while the respective activation entropies were found to be 15 ± 3 and 17 ± 3 eu (from rates measured at temperatures between 107 and 126 °C and 57 and 79 °C, respectively). These olefin dissociation rates are in fact much slower than those of the corresponding ($^{t\mathrm{Bu}}$PCP)Ir complexes. Nevertheless, extrapolation to 125 °C for *trans*-2-hexene self-exchange (experimentally determined at increments from 57 to 79 °C) affords a rate of 2.1×10^2 s^{-1}, which is independent of excess olefin concentration and still much faster than the isomerization of ($^{t\mathrm{Bu}}$POCOP)Ir(*trans*-2-hexene) to ($^{t\mathrm{Bu}}$POCOP)Ir(1-hexene) (discussed below). Thus, at present, we have no good explanation for the curvature seen in the plot of Figure 2 (and the rate dependence on [1-alkene] which it implies), but we note that it is fully reproducible.

In view of the above, we cannot assign a meaningful rate constant or activation parameters to the ($^{t\mathrm{Bu}}$POCOP)Ir-catalyzed isomerization of α-olefins. Importantly, however, the rate is not significantly faster than that of olefin isomerization catalyzed by ($^{t\mathrm{Bu}}$PCP)Ir; indeed, it is somewhat slower at the low concentrations of olefin present during typical AM experiments. Thus, quite surprisingly, the difference between these two catalysts in the product distribution obtained from alkane metathesis apparently does not result from a difference in olefin isomerization rates. In view of these results, we have begun to investigate in detail the regioselectivity of dehydrogenation by these two catalysts. Indeed, preliminary results indicate that ($^{t\mathrm{Bu}}$POCOP)Ir shows much less selectivity than either ($^{t\mathrm{Bu}}$PCP)Ir or ($^{i\mathrm{Pr}}$PCP)Ir for dehydrogenation at the terminal position of the *n*-alkanes.[26]

Intramolecular H/D Scrambling. A sample of ($^{t\mathrm{Bu}}$POCOP)Ir(propene-d_3) (**3-d_3**) was prepared containing a deuterium-labeled methyl group in the propene ligand. Monitoring a mesitylene-d_{12} solution of **3-d_3** by ^{1}H NMR revealed no H/D exchange at room temperature over the course of 24 h. However, heating the solution at 60 °C resulted in H/D scrambling between the methyl group and the terminal carbon of propene (Scheme 6 and Figure 3). The reaction approaches equilibrium with a half-life of ca. 9 h, corresponding to a free energy of activation, $\Delta G^{\ddagger}$, of ca. 26.7 kcal/mol. Increasing the temperature to 125 °C significantly increases the rate, and the reaction reaches equilibrium in ca. 10 min (cf. comparable rates, on the order of 0.2 catalytic turnover/min, observed for α-olefin isomerization catalyzed by either ($^{t\mathrm{Bu}}$POCOP)Ir or ($^{t\mathrm{Bu}}$PCP)Ir).

The H/D exchange is proposed to occur via the Ir(III) allyl deuteride/hydride intermediate, **4-d_3**, in Scheme 6. As in the case with α-olefin noted above (in either alkane or arene solvent), in the presence of excess propene, no iridium dihydride is observable. Since mesitylene was used as solvent in this experiment, there would be even less dihydride present than if the solvent were alkane (cf. eq 2).

Insertion mechanisms for isomerization involve the addition of a hydride derived from one olefin molecule to the double bond of a second olefin molecule; that is, the mechanism is

Scheme 6. Hydrogen/Deuterium Scrambling via an Ir(III) η^3-Allyl Hydride Intermediate

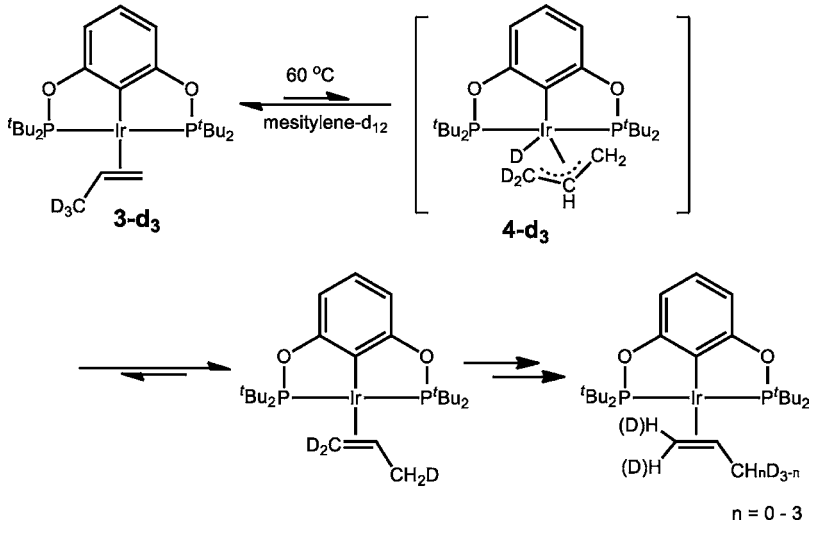

dx.doi.org/10.1021/ja301464c | J. Am. Chem. Soc. 2012, 134, 13276−13295

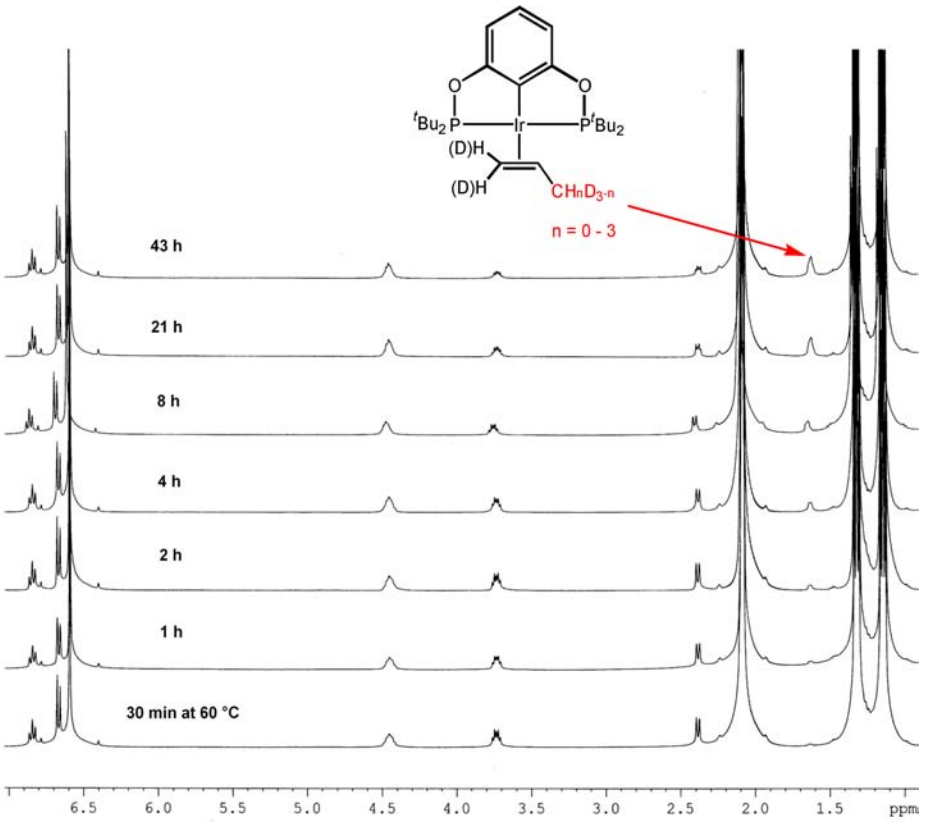

Figure 3. ^{1}H NMR overlay showing the H/D scrambling between the methyl and methylene sites of the propene ligand in **3-d_3**.

Scheme 7. Ligand Exchange Reaction of 3-d_6 and Propene

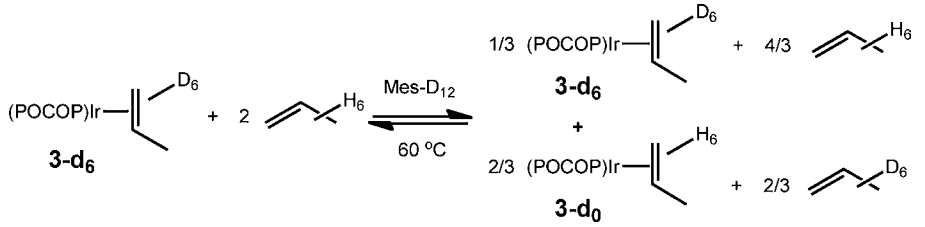

Scheme 8. H/D Scrambling at the Central Carbon of Propene Involving a Metallacyclobutane Intermediate

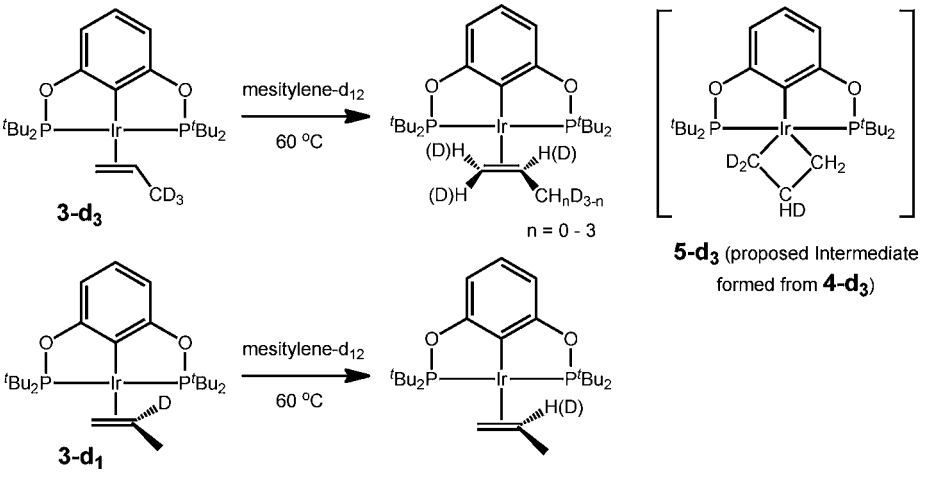

intermolecular in contrast to the allyl mechanism in which a hydride effectively undergoes an intramolecular 1,3 shift. With this in mind, ($^{t\text{Bu}}$POCOP)Ir(propene-d_6) (**3-d_6**) was treated with 2 equiv of free perprotio-propene in mesitylene-d_{12} at 60 °C (Scheme 7). If an iridium hydride/deuteride species were present in the system and "isomerization" (degenerate 1,2 shift

dx.doi.org/10.1021/ja301464c | J. Am. Chem. Soc. 2012, 134, 13276−13295

Scheme 9. Formation of (POCOP)Ir(H)(η^3-Allyl) and (POCOP)Ir(η^2-Propene)

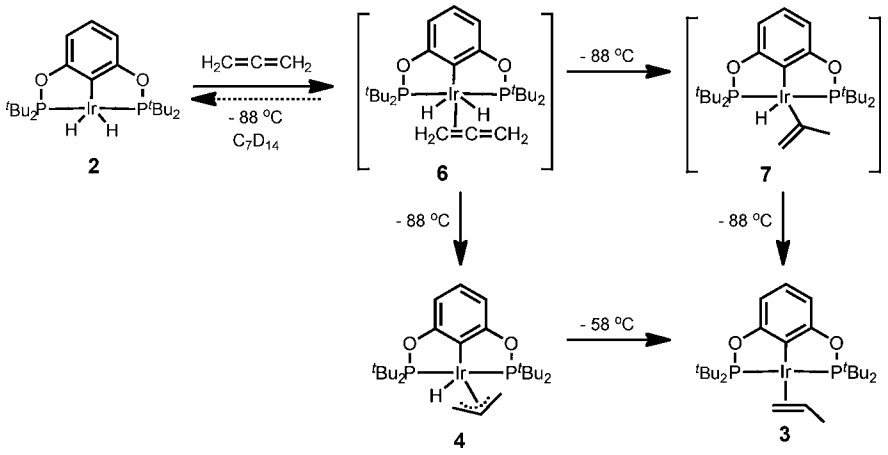

of the double bond) proceeded through a hydride addition mechanism, then intermolecular H/D scrambling would occur. However, only ligand exchange was observed in this experiment. Complex **3-d_6** underwent ligand substitution with propene ($t_{1/2}$ ca. 1 h, 60 °C), giving a mixture of 1/3 equiv of **3-d_6** and 2/3 equiv of **3-d_0**, as well as 2/3 equiv of propene-d_6 and 4/3 equiv of propene-d_0 (the expected statistical ratio of products; Scheme 7). No crossover of H/D between the perdeuterio and perprotio species occurred under the reaction conditions after 24 h. These results strongly argue against the hydride addition mechanism for the H/D exchange reaction, while a π-allyl mechanism, as shown in Scheme 6, fully accounts for the intramolecular H/D scrambling.

Interestingly, in addition to the H/D exchange between the propene terminal vinyl and methyl positions, we also observed deuterium incorporation into the central methine position in the ($^{t\text{Bu}}$POCOP)Ir(propene-d_3) (**3-d_3**) (Scheme 8 and Figure 3). This scrambling process is revealed more clearly upon thermolysis of **3-d_1** (deuterium-substituted at the central methine site, Scheme 8). Heating of this d_1 species in mesitylene at 60 °C resulted in incorporation of ^{1}H into the central site with a half-life of ca. 230 h (Scheme 8 and Figure 19 in Experimental Details). This rate is substantially slower than the H/D exchange between the terminal carbon sites ($t_{1/2}$ = ca. 9 h). The reaction presumably proceeds via a metallacyclobutane intermediate (**5**), as depicted in Scheme 8. Similar iridium(III) metallacyclobutane species have been reported by Bergman,[27] Ibers,[28] and Stryker.[29]

Observation of an Ir(III) η^3-Allyl Hydride Intermediate. The intramolecular H/D exchange reactions are fully consistent with a π-allyl olefin isomerization mechanism. In addition, the key intermediate in this isomerization, the Ir(III) η^3-allyl hydride species (**4**), has been generated separately and characterized by low-temperature NMR techniques. Treatment of dihydride complex **2** with allene (5 equiv) in methylcyclohexane-d_{14} at −88 °C generated 18% of hydrido(allyl) complex **4** and 82% of propene complex **3** (Scheme 9). The characteristic ^{1}H NMR data for complex **4** include a hydride resonance at δ −13.1 ppm (triplet, $^2J_{\text{P–H}}$ = 15.0 Hz) and five separate H signals for the allyl unit H_{anti}, 2.0, 2.1; H_{syn}, 2.6, 2.8; H_2, 4.9 ppm. The ^{31}P NMR spectrum shows a pair of AB pattern doublets at 158.5 and 152.5 ppm ($^2J_{\text{P–P}}$ = 341 Hz) for two inequivalent phosphorus nuclei. The 1:5 ratio of complexes **4** and **3** is constant throughout the course of their formation from **2** and persists unchanged for hours in solution at −88 °C. Complex **4** rearranges quantitatively to **3** but only at higher temperature, indicating that these two species are kinetic products and that, at −88 °C, **3** and **4** form via independent routes. We propose that at −88 °C **4** is formed via 1,2 insertion of allene complex **6** and that **3** is formed by 2,1 insertion to yield **2**-propenyl hydride **7**, followed by reductive elimination (Scheme 9). Allene complex **6** is undetected during the reaction, so it cannot be determined whether it is formed reversibly or if its formation is rate-determining in producing **4** and **3**.

When the mixture was warmed to −58 °C, **4** rearranged to form **3** through the migration of the hydride to the terminal carbon. The reaction is first-order with a rate constant of 5×10^{-4} s^{-1}, corresponding to $\Delta G^{\ddagger}$ = 15.6 kcal/mol. A similar hydrido(η^3-allyl)iridium(III) complex, (η^5-C_5Me_5)IrH(η^3-allyl), has been reported by McGhee and Bergman.[27] In contrast to **4**, this hydrido(allyl) complex is thermally stable and could be isolated; the 16-electron complex (η^5-C_5Me_5)Ir(propene) was postulated as a reversibly formed intermediate in the oxidative addition of benzene to the iridium(I) center formed reversibly from the η^3-allyl hydride.[27] The observation of the allyl hydride species **4** and its rapid rearrangement to propene complex **3** provides additional evidence in support of a π-allyl olefin isomerization mechanism.

Stoichiometric Isomerization of Coordinated 2-Alkene to 1-Alkene. Closely related to the 1,3-H(D) shift observed for coordinated propene, stoichiometric and apparently intramolecular isomerizations of hexene were observed with both ($^{t\text{Bu}}$PCP)Ir and ($^{t\text{Bu}}$POCOP)Ir complexes. Interestingly, the isomerizations proceed in the reverse of the direction thermodynamically favored for the free olefins.

At 60 °C, ($^{t\text{Bu}}$POCOP)Ir(η^2-*trans*-2-hexene) underwent isomerization in *p*-xylene solvent to give ($^{t\text{Bu}}$POCOP)Ir(1-hexene). Free *trans*-2-hexene is more stable than 1-hexene by ca. 2.5 to 3 kcal/mol.[30] The difference in their binding enthalpies must therefore exceed that value; presumably, this is driven by decreased crowding in the 1-hexene complex. The reaction kinetics were monitored by ^{31}P NMR spectroscopy and a first-order rate constant of 5.6×10^{-6} s^{-1} was obtained using COPASI[31] kinetics fitting software (Figure 4). The rate of the ($^{t\text{Bu}}$POCOP)Ir(*trans*-2-hexene) isomerization is somewhat slower than, but quite comparable to, that of 1,3-D migration of ($^{t\text{Bu}}$POCOP)Ir(propene-d_3), which has a rate constant of ca. 2.1×10^{-5} s^{-1} at 60 °C. An Eyring plot of isomerization rates of ($^{t\text{Bu}}$POCOP)Ir(*trans*-2-hexene) to ($^{t\text{Bu}}$POCOP)Ir(1-hexene), based on rates measured at 10 degree increments from 60 to

dx.doi.org/10.1021/ja301464c | J. Am. Chem. Soc. 2012, 134, 13276−13295

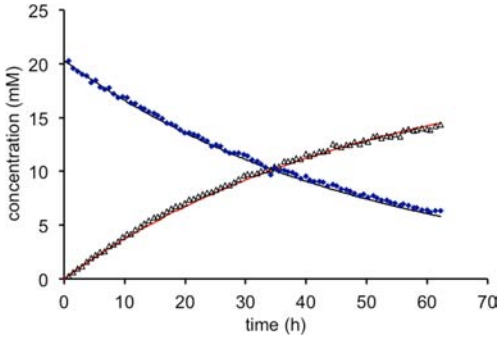

Figure 4. Isomerization of ($^{t\text{Bu}}$POCOP)Ir(*trans*-2-hexene) to ($^{t\text{Bu}}$POCOP)Ir(1-hexene) at 60 °C; curve shown represents a best fit to a first-order rate constant of 5.6×10^{-6} s^{-1} obtained using COPASI[31] kinetics fitting software.

90 °C, gave activation parameters $\Delta H^{\ddagger}$ = 23.7(±0.7) kcal/mol and $\Delta S^{\ddagger}$ = −9.3(±1.1) eu (Figure 5).

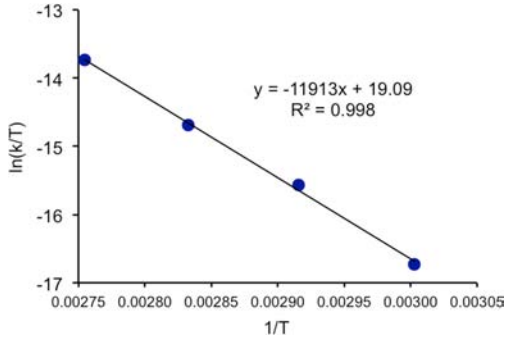

Figure 5. Eyring plot for the isomerization of ($^{t\text{Bu}}$POCOP)Ir(*trans*-2-hexene) to ($^{t\text{Bu}}$POCOP)Ir(1-hexene) in the temperature interval 60 to 90 °C.

The analogous isomerization reaction of ($^{t\text{Bu}}$PCP)Ir(*trans*-2-hexene) was also observed, and its kinetics were monitored. As noted above, at 60 °C, dissociation of 1-hexene and *trans*-2-hexene from ($^{t\text{Bu}}$PCP)Ir is rapid on the NMR time scale, resulting in broadening of the ^{31}P NMR signals and impeding kinetics measurements. The kinetics could be measured at 25 °C, however, and a first-order rate constant of $3.2(\pm0.4) \times 10^{-5}$ s^{-1} was obtained (Figure 6), corresponding to $\Delta G^{\ddagger}$ = 23.6 kcal/mol. This compares with the kinetics of isomerization of the ($^{t\text{Bu}}$POCOP)Ir analogue, which can be extrapolated to 25 °C (based on the Eyring plot of Figure 5) to give a value of 2.5×10^{-7} s^{-1} (2 orders of magnitude slower).

If we assume the same value of $\Delta S^{\ddagger}$ for the ($^{t\text{Bu}}$PCP)Ir(*trans*-2-hexene) and ($^{t\text{Bu}}$POCOP)Ir(*trans*-2-hexene) isomerizations, the rate of the ($^{t\text{Bu}}$PCP)Ir(*trans*-2-hexene) isomerization extrapolates to ca. 0.3 s^{-1} at 125 °C, with $\Delta G^{\ddagger}$ = 24.5 kcal/mol. This compares with the rate of isomerization of 1-hexene to *trans*-2-hexene, *catalyzed* by ($^{t\text{Bu}}$PCP)Ir, 4.2×10^{-3} s^{-1} at 125 °C, corresponding to a barrier of $\Delta G^{\ddagger}$ = 27.9 kcal/mol. The somewhat greater free energy of activation for the isomerization of 1-hexene to *trans*-2-hexene is consistent with our general mechanistic picture which proposes (Scheme 4) that the catalytic reaction proceeds via isomerization of ($^{t\text{Bu}}$PCP)Ir(1-hexene) to ($^{t\text{Bu}}$PCP)Ir(*trans*-2-hexene). This step must be endergonic by several kcal/mol since the reverse (stoichiometric) reaction proceeds to apparent completion; therefore, the free energy barrier of the forward (catalytic) reaction must be several kcal/mol

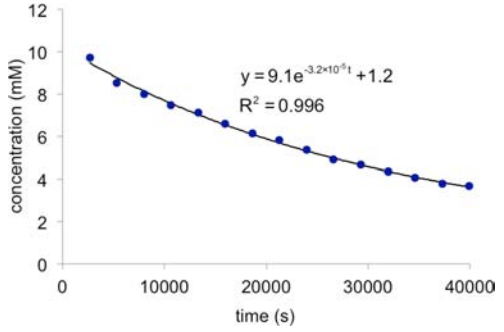

Figure 6. Isomerization of ($^{t\text{Bu}}$PCP)Ir(*trans*-2-hexene) to ($^{t\text{Bu}}$PCP)Ir-(1-hexene) at 25 °C.

greater than that of the stoichiometric reaction. Note that under catalytic conditions the presumed uphill isomerization of bound 1-hexene is followed by the very rapid loss of *trans*-2-hexene (extrapolated to a rate of ca. 2×10^{4} s^{-1} at 125 °C) and then addition of free 1-hexene.

As will be discussed in detail below, the most significant difference between the ($^{t\text{Bu}}$PCP)Ir and ($^{t\text{Bu}}$POCOP)Ir fragments appears to be greater crowding in the former. The fact that isomerization of bound *trans*-2-hexene proceeds more rapidly in the case of ($^{t\text{Bu}}$PCP)Ir therefore suggested that the rate-determining transition states are less crowded than the ground states (the olefin π-complexes). In this context, we investigated the effect of increasing the steric demands of the olefin substrate by monitoring the isomerization kinetics of a bound branched olefin, *trans*-4-methylpent-2-ene (MP-2-ene).

($^{t\text{Bu}}$POCOP)Ir(MP-2-ene) was found to undergo isomerization to the 4-methyl-1-pentene complex ($^{t\text{Bu}}$POCOP)Ir(MP-1-ene) (eq 3, X = O) analogously to the isomerization of

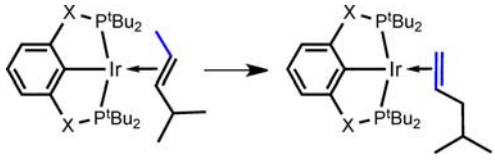

(3)

($^{t\text{Bu}}$POCOP)Ir(*trans*-2-hexene).Under the same conditions as the reaction of the 2-hexene complex (60 °C, *p*-xylene solution), the kinetics of the MP-2-ene complex were monitored and the reaction was found to proceed with a first-order rate constant of 5×10^{-4} s^{-1} (Figure 7), ca. 90-fold faster than the reaction of the *trans*-2-hexene complex. Assuming that the two complexes undergo isomerization through analogous pathways, the greater rate of the branched olefin complex provides further evidence that the rate-determining transition states are sterically less demanding than the respective olefin π-complex reactants.

Analogously, ($^{t\text{Bu}}$PCP)Ir(MP-2-ene) underwent isomerization to give ($^{t\text{Bu}}$PCP)Ir(MP-1-ene) (eq 3, X = CH_2) with a rate constant of 7.9×10^{-5} s^{-1} at 25 °C (Figure 8). This also is more rapid than isomerization of the respective linear olefin complex, ($^{t\text{Bu}}$PCP)Ir(*trans*-2-hexene), although only by a factor of 2.5.

COMPUTATIONAL STUDIES AND MECHANISTIC ANALYSIS

The isomerization or double-bond migrations discussed above were modeled with DFT calculations[32] using two of the most widely applied functionals in transition metal chemistry, PBE[33]

dx.doi.org/10.1021/ja301464c | J. Am. Chem. Soc. 2012, 134, 13276−13295

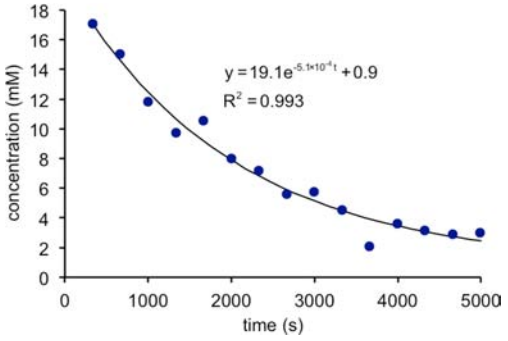

Figure 7. Isomerization of ($^{t\text{Bu}}$POCOP)Ir(MP-2-ene) to ($^{t\text{Bu}}$POCOP)-Ir(MP-1-ene) at 60 °C.

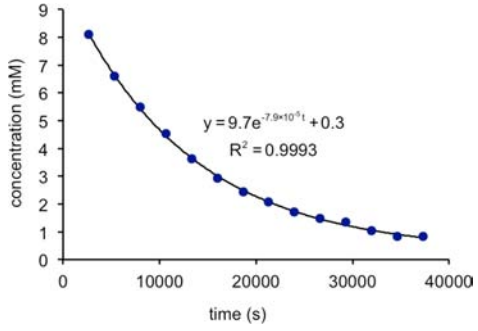

Figure 8. Isomerization of ($^{t\text{Bu}}$PCP)Ir(MP-2-ene) to ($^{t\text{Bu}}$PCP)Ir(MP-1-ene) at 25 °C.

and M06[34] (see Computational Methods for a full description). The PBE functional contains pure DFT functionals based on the generalized gradient approximation (GGA); it is parameter independent, very robust, and efficient. The more recently developed M06 functional is a hybrid functional (28% exact exchange), includes kinetic energy and dispersion corrections, and is partially parametrized against experimental data. Calculations were conducted on the reactions of ($^{t\text{Bu}}$PCP)Ir and ($^{t\text{Bu}}$POCOP)Ir fragments with propene, 1-hexene/*trans*-2-hexene, and MP-1-ene/MP-2-ene.

The two different functionals employed here generally yielded similar results with respect to the *relative* energies of the different pathways investigated, but the PBE functional appeared to afford considerably better agreement with those absolute values that could be determined experimentally. For example, using the PBE functional, the enthalpies of olefin binding, $\Delta H°$, for ($^{t\text{Bu}}$PCP)Ir(1-hexene), ($^{t\text{Bu}}$PCP)Ir(*trans*-2-hexene), ($^{t\text{Bu}}$POCOP)Ir(1-hexene), and ($^{t\text{Bu}}$POCOP)Ir(*trans*-2-hexene) were calculated to be 20.6, 12.7, 29.6, and 24.8 kcal/mol, respectively, while M06 gave values of 30.1, 24.5, 36.9, and 35.0 kcal/mol (Table 1). As noted above, the activation enthalpies for dissociation of the olefins from the (pincer)Ir fragments were determined experimentally, by EXSY NMR spectroscopy. Assuming that the reverse reaction, olefin addition, has a positive enthalpy of activation, the (thermodynamic) enthalpies of binding must be less than the activation enthalpies of dissociation. Indeed, the correlation of experimental values of $\Delta H^{‡}$ with PBE-based values of $\Delta H°$ is striking; in all four cases, the experimental $\Delta H^{‡}$ for dissociation is greater, by less than 3 kcal/mol, than the calculated value of $\Delta H°$, consistent with an expectedly small but positive value of $\Delta H^{‡}$ for olefin addition to (pincer)Ir. In contrast, the M06-based binding enthalpies are significantly *greater* (by 7−9 kcal/mol) than the experimental activation enthalpies, most likely as the result of overestimating the strength of Ir−olefin π-interactions and/or underestimating the strength of steric interactions.

Table 1. Experimental and Calculated Parameters for Olefin Dissociation from Complexes of ($^{t\text{Bu}}$PCP)Ir and ($^{t\text{Bu}}$POCOP)Ir

olefin complex	$\Delta H^{‡}$ (exp)	$\Delta H°$ (PBE)	$\Delta H°$ (M06)
($^{t\text{Bu}}$PCP)Ir(1-hexene)	21.4	20.6	30.1
($^{t\text{Bu}}$PCP)Ir(*trans*-2-hexene)	15.4	12.7	24.5
($^{t\text{Bu}}$POCOP)Ir(1-hexene)	29.4	29.6	36.9
($^{t\text{Bu}}$POCOP)Ir(*trans*-2-hexene)	26.0	24.8	35.0

An accurate calculation of the energies of the π-complexes is obviously important in obtaining reaction energies and modeling kinetics, as the π-complexes are the resting state or reagent in all of the isomerizations. Moreover, the superiority of PBE in such calculations might well be expected to extrapolate to the various intermediates and transition states in the isomerization pathways since these species may have much in common with the olefin complexes. In this section, we will therefore refer exclusively to values calculated using the PBE functional. For all systems studied, however, calculations using the M06 functional were also performed, and those results can be found in Supporting Information. Importantly, the results obtained with either functional support the same overarching conclusions regarding the preferred isomerization pathway.

As noted above, the experimental kinetics of 1-octene isomerization catalyzed by ($^{t\text{Bu}}$POCOP)Ir show a clear positive dependence on 1-octene concentration, contrary to the proposed mechanism for isomerization by ($^{t\text{Bu}}$PCP)Ir (Scheme 4). As such, calculations for a proposed mechanism for catalytic isomerization by ($^{t\text{Bu}}$POCOP)Ir may not be applicable to the actual mechanism of isomerization by ($^{t\text{Bu}}$POCOP)Ir. Accordingly, calculations for the ($^{t\text{Bu}}$POCOP)Ir system are presented below primarily for comparison with ($^{t\text{Bu}}$PCP)Ir.

Hydride Addition Mechanism. The pathways for 1-hexene isomerization via the hydride mechanism for both ($^{t\text{Bu}}$POCOP)Ir and ($^{t\text{Bu}}$PCP)Ir (Scheme 3) were calculated using DFT. The calculations indicate that the barrier to the hydride pathway for isomerization is prohibitively high, in accord with the body of experimental results discussed above arguing against a hydride mechanism for double-bond migration. The barrier to insertion of olefin into the Ir−H bonds, to give (pincer)Ir(alkyl)(H), was found to be quite high ($\Delta G^{‡}$ > 30 kcal/mol for both ($^{t\text{Bu}}$POCOP)Ir and ($^{t\text{Bu}}$PCP)Ir and for propene and 1-hexene), but the highest (rate-determining) barrier was found for subsequent rotation of the alkyl group about the Ir−C bond with calculated free energy barriers >40 kcal/mol above the corresponding η^2-olefin complexes (44.7 and 46.3 kcal/mol for ($^{t\text{Bu}}$PCP)Ir complexes of propene and 1-hexene, respectively). By contrast, the experimental value obtained for catalytic isomerization of 1-hexene by ($^{t\text{Bu}}$PCP)Ir was found to be $\Delta G^{‡}$ = 27.9 kcal/mol, while the experimental value for the stoichiometric isomerization of ($^{t\text{Bu}}$PCP)Ir(*trans*-2-hexene) to ($^{t\text{Bu}}$PCP)Ir(1-hexene) at 25 °C was $\Delta G^{‡}$ = 23.6 kcal/mol. A more detailed treatment of the hydride pathway (including calculations for propene isomerization) can be found in Supporting Information.

Comparison of PCP and POCOP Complexes: Steric Effects. Although both ($^{t\text{Bu}}$PCP)Ir and ($^{t\text{Bu}}$POCOP)Ir complexes show prohibitively high barriers for the hydride

dx.doi.org/10.1021/ja301464c | J. Am. Chem. Soc. 2012, 134, 13276−13295

addition pathway, there are significant differences between the two in the factors determining the barrier magnitudes. In particular, (^{tBu}POCOP)IrH$_2$ is ca. 5 kcal/mol higher in free energy than (^{tBu}PCP)IrH$_2$, relative to their respective propene or 1-hexene complexes. This accounts for the observation that under alkane metathesis conditions (^{tBu}POCOP)Ir is only observable as the olefin complex, while (^{tBu}PCP)Ir is only observable as the dihydride. An investigation into the origin of this difference, detailed below, leads to the conclusion that it is largely due to steric factors.

Although the two (pincer)Ir fragments are formally isostructural, a comparison of the geometries of (^{tBu}PCP)Ir and (^{tBu}POCOP)Ir complexes reveals significant differences. The smaller size of the O-linker versus CH$_2$ combined with the tendency of O to form shorter bonds but greater bond angles results in the phosphino groups being "pulled back" in (^{tBu}POCOP)Ir. Thus, for the free (pincer)Ir fragments, the calculated C$_{aryl}$–O and O–P bond lengths are 1.39 and 1.71 Å, respectively, in (^{tBu}POCOP)Ir, whereas the C$_{aryl}$–CH$_2$ and CH$_2$–P bond lengths in (^{tBu}PCP)Ir are longer at 1.51 and 1.86 Å, respectively (Scheme 10). The C$_{aryl}$–O–P bond angle

Scheme 10. Selected Distances (Å) and Angles in Calculated Structures of (^{tBu}PCP)Ir and (^{tBu}POCOP)Ir

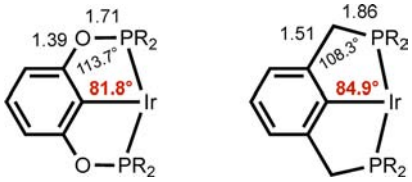

is 113.7° in (^{tBu}POCOP)Ir, whereas the C$_{aryl}$–CH$_2$–P angle is 108.3° in (^{tBu}PCP)Ir. These differences lead to smaller C$_{aryl}$–Ir–P angles in (^{tBu}POCOP)Ir (81.8°) as compared with 84.9° in (^{tBu}PCP)Ir. Thus, the P–Ir–P angle is calculated to be approximately 6° smaller in (^{tBu}POCOP)Ir than in (^{tBu}PCP)Ir (163.6 vs 169.9°, respectively).

Experimental values for various (^{tBu}POCOP)Ir and (^{tBu}PCP)-Ir complexes indeed reveal slightly greater P–Ir–P angles for the latter. For example, (^{tBu}POCOP)IrHCl[35] and (^{tBu}PCP)-IrHCl[36] complexes have P–Ir–P angles of 159.79(5) and 164.27(4)°, while the corresponding dinitrogen complexes have P–Ir–P angles of 154.86(3)[37] and 160.22(10)°,[38] respectively. While these structural differences may not seem large, the resulting gap between the bulky phosphino-*t*-butyl groups is substantially less in (^{tBu}PCP)Ir than in (^{tBu}POCOP)Ir in the region of the open coordination site (the site opposite to the pincer aryl group). The closest distances between hydrogens of the two phosphino groups flanking the vacant coordination sites in (^{tBu}PCP)Ir and (^{tBu}POCOP)Ir are 3.01 and 4.43 Å, respectively (Scheme 11). Taking the van der Waals radius of hydrogen as 1.2 Å[39,40] would suggest a space of only 0.61 Å between the corresponding van der Waals surfaces in (^{tBu}PCP)Ir.

As a result of the small gap between the *trans*-di-*t*-butyl-phosphino groups of (^{tBu}PCP)Ir, addition of even the smallest substrate, H$_2$, results in a complex with four contacts (2.288, 2.289, 2.331, 2.332 Å) between *t*-Bu hydrogen atoms and the resulting hydrides that are less than twice the van der Waals radius of hydrogen, suggesting that even H$_2$ addition to (^{tBu}PCP)Ir might be disfavored by steric crowding (Scheme 12). In contrast, in (^{tBu}POCOP)IrH$_2$, there are only two short H–H

Scheme 11. Space-Filling Models of Calculated Structures of (^{tBu}PCP)Ir and (^{tBu}POCOP)Ir with Closest H–H Distances Indicated

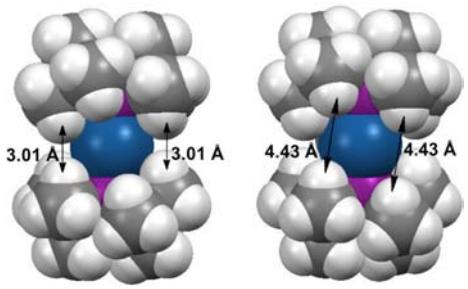

Scheme 12. Space-Filling Models of Calculated Structures of (^{tBu}PCP)IrH$_2$ and (^{tBu}POCOP)IrH$_2$ (Ir-Bound Hydrides Yellow) with H(^{t}Bu)–H(Hydride) Distances Indicated

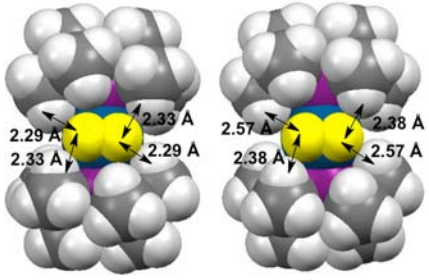

distances (both 2.384 Å, just barely below 2.4 Å), indicating that if there is any crowding in (^{tBu}POCOP)IrH$_2$ it is significantly less than in (^{tBu}PCP)IrH$_2$.

In order to further probe the energetic effects of crowding, we considered complexes in which the pincer *t*-Bu groups were replaced with methyl groups (Table 2). The enthalpy of addition of H$_2$ to (^{Me}PCP)Ir and (^{Me}POCOP)Ir differs very little from that of the *t*-Bu analogues. Moreover, the small difference between the Me and *t*-Bu analogues is essentially equal for ^{R}PCP and ^{R}POCOP complexes (1.2 and 1.1 kcal/mol favoring addition to the complexes where R = Me). We conclude that there is no significant steric contribution to the energetics of H$_2$ addition to either complex. Given the short H–H nonbonding distances in (^{tBu}PCP)IrH$_2$, it seems that H$_2$ just barely "fits" into the cleft between the opposing (^{tBu}PCP)Ir phosphino-*t*-butyl groups; this would suggest that addition of any substrate larger than H$_2$ to (^{tBu}PCP)Ir would result in significant crowding and more so than in the case of addition to (^{tBu}POCOP)Ir.

Accordingly, whereas H$_2$ adds to (^{Me}PCP)Ir slightly more favorably than to (^{tBu}PCP)Ir (by 1.2 kcal/mol), the addition of 1-hexene to (^{tBu}PCP)Ir is 13.8 kcal less favorable than to (^{Me}PCP)Ir, indicative of very significant crowding. Addition of 1-hexene to (^{tBu}POCOP)Ir is likewise less favorable than to the ^{Me}POCOP complex, but only by 9.2 kcal/mol. These results suggest that crowding is important in both (^{tBu}PCP)Ir and (^{tBu}POCOP)Ir 1-hexene complexes, but the penalty is about 4.6 kcal/mol greater for (^{tBu}PCP)Ir. Accordingly, addition of H$_2$ to (^{tBu}PCP)Ir is 8.4 kcal/mol more favorable than 1-hexene addition, while the corresponding value is 3.6 kcal/mol for (^{tBu}POCOP)Ir (eq 4). This difference of 4.8 kcal/mol (or 5.4 kcal/mol for the propene complexes; see Figure 9) can thus

$$\text{(pincer)Ir(1-hexene)} + \text{H}_2 \rightleftharpoons \text{(pincer)IrH}_2 + \text{1-hexene} \quad \begin{matrix}\text{pincer} = {}^{tBu}\text{PCP};\ \Delta H = -8.4\ \text{kcal/mol} \\ \text{pincer} = {}^{tBu}\text{POCOP};\ \Delta H = -3.6\ \text{kcal/mol}\end{matrix} \quad (4)$$

dx.doi.org/10.1021/ja301464c | J. Am. Chem. Soc. 2012, 134, 13276–13295

Table 2. Calculated Thermodynamic Parameters for Addition of H_2 and Hexenes to (^{R}PCP)Ir and (^{R}POCOP)Ir, R = ^{t}Bu, Me, and H[a]

addition product	ΔE	ΔH	ΔG	ΔS
(^{tBu}PCP)IrH$_2$	−31.2	−29.0	−20.3	−29.2
(^{tBu}PCP)Ir(1-hexene)	−22.9	−20.6	−5.3	−51.9
(^{tBu}PCP)Ir(*trans*-2-hexene)	−15.0	−12.7	2.6	−51.3
(^{Me}PCP)IrH$_2$	−32.0	−30.2	−21.9	−27.8
(^{Me}PCP)Ir(1-hexene)	−35.4	−34.4	−21.2	−44.3
(^{Me}PCP)Ir(*trans*-2-hexene)	−33.2	−32.2	−18.5	−46.1
(^{H}PCP)IrH$_2$	−31.2	−29.4	−21.2	−27.6
(^{H}PCP)Ir(1-hexene)	−36.8	−35.7	−23.2	−42.5
(^{H}PCP)Ir(*trans*-2-hexene)	−35.1	−34.0	−21.3	−42.9
(^{tBu}POCOP)IrH$_2$	−35.3	−33.2	−24.9	−27.9
(^{tBu}POCOP)Ir(1-hexene)	−31.4	−29.6	−15.2	−48.4
(^{tBu}POCOP)Ir(*trans*-2-hexene)	−27.2	−24.8	−8.9	−53.3
(^{Me}POCOP)IrH$_2$	−36.2	−34.3	−25.8	−28.4
(^{Me}POCOP)Ir(1-hexene)	−40.0	−38.8	−26.1	−42.7
(^{Me}POCOP)Ir(*trans*-2-hexene)	−38.1	−37.0	−23.8	−44.4
(^{H}POCOP)IrH$_2$	−36.3	−34.4	−25.8	−28.9
(^{H}POCOP)Ir(1-hexene)	−42.5	−41.3	−28.6	−42.8
(^{H}POCOP)Ir(*trans*-2-hexene)	−41.4	−40.4	−27.2	−44.1

[a]Units are kcal/mol for ΔE, ΔH, and ΔG; units are cal/(deg-mol) for ΔS.

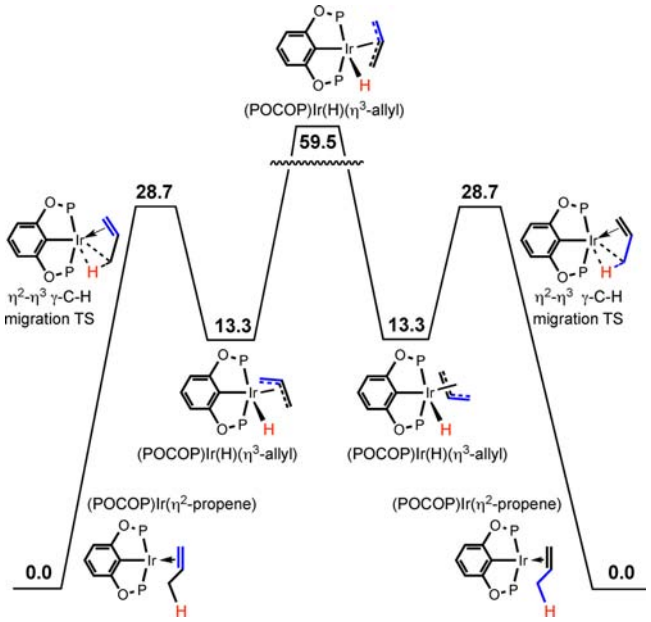

Figure 9. An η^2-η^3 rotation pathway (γ-H migration) calculated for 1,3-H migration in (^{tBu}POCOP)Ir(η^2-propene).

be attributed solely to steric effects. It should be emphasized that, as indicated above, in the absence of steric factors, (^{R}POCOP)Ir fragments add *both* olefins and hydrogen more favorably than (^{R}PCP)Ir fragments do,[41] by ca. 5 kcal/mol, but these electronic factors do not contribute to the *greater relative preference for olefins versus* H_2 that is demonstrated by (^{tBu}POCOP)Ir versus (^{tBu}PCP)Ir.

In accord with the above considerations, addition of *trans*-2-hexene to (^{tBu}PCP)Ir is 19.5 kcal/mol less favorable than addition to (^{Me}PCP)Ir, while the difference between *t*-Bu and Me analogues is only 12.2 kcal/mol for (^{R}POCOP)Ir. This suggests that crowding is ca. 7 kcal/mol more severe in (^{tBu}PCP)Ir(*trans*-2-hexene) than in (^{tBu}POCOP)Ir(*trans*-2-hexene).

The significantly greater steric crowding in (^{tBu}PCP)Ir versus (^{tBu}POCOP)Ir complexes presumably has important implications in any comparison of the two fragments and indeed in almost any reaction involving (^{tBu}PCP)Ir complexes in particular.

Allyl Mechanism for Olefin Isomerization. Isomerization mechanisms proceeding through η^3-allyl intermediates, while often proposed to be operative,[1,2,10−14] have not been the subject of thorough mechanistic studies or even detailed mechanistic proposals. Formation of the η^3-allyl hydride is generally assumed to proceed via γ-hydride migration from a π-coordinated olefin; we will refer to this as an η^2-η^3 step. If the resulting η^3-allyl ligand is symmetrical or approximately symmetrical with respect to the hydride, migration of the hydride to the terminal carbon C_b (Scheme 13a) is equivalent to the reverse of the η^2-η^3 step and results in double-bond migration.

Scheme 13. Schematic Illustration of the π-Allyl Pathway for Olefin Isomerization Proceeding via Formation of an Allyl Ligand That Is (a) Symmetrical or (b) Unsymmetrical with Respect to the Hydride

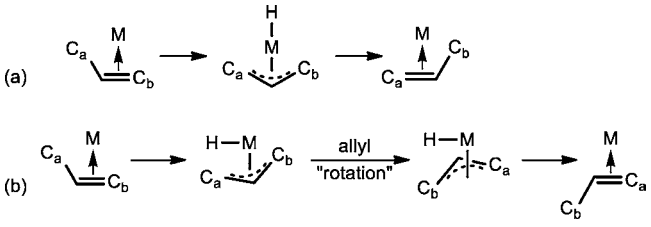

Alternatively, however, the hydride may be located to one "side" of the resulting allyl in such a way that it can migrate only to the same terminal carbon to which it was originally bound, that is, terminal carbon C_a (Scheme 13b), thus requiring one or more additional rearrangement steps in order to effect a net double-bond migration. The calculations clearly indicate that the allyl carbons of the (pincer)Ir(η^3-allyl)(H) complexes are inequivalent in this sense with respect to the hydride, in accord with the spectroscopic characterization of (^{tBu}POCOP)Ir(η^3-allyl)(H) (**4**).

Conceptually, the simplest rearrangement of the η^3-allyl ligand that would permit subsequent migration of the hydride to the γ-carbon would be a 180° rotation during which the allyl group remains bound in an η^3 fashion. Such a process has in fact been well-established by fluxional NMR studies.[42,43] Our calculations indicate, however, that the barriers for such a rotation in the pincer−Ir systems are prohibitively high, 59.5 kcal/mol for (^{tBu}POCOP)Ir(η^3-propenyl)(H) (Figure 9) and 41.0 kcal/mol for (^{tBu}PCP)Ir(η^3-propenyl)H. (In the latter case, the reaction proceeds through Ir−P bond cleavage, which is facilitated by relief of severe steric crowding in the (^{tBu}PCP)Ir((η^3-allyl)H intermediate.) For isomerization of 1-hexene by (^{tBu}POCOP)Ir, the barrier was calculated to be even higher, 62.4 kcal/mol, while we were unable to locate a TS for rotation of the corresponding (^{tBu}PCP)Ir intermediate.

An alternative pathway that would effect a net "rotation" of the allyl group could proceed via an initial η^3-η^1 "opening" of the η^3-allyl ligand, followed by rotation around the resulting iridium−carbon σ-bond, and terminated by η^1-η^3 "closing", as

dx.doi.org/10.1021/ja301464c | J. Am. Chem. Soc. 2012, 134, 13276−13295

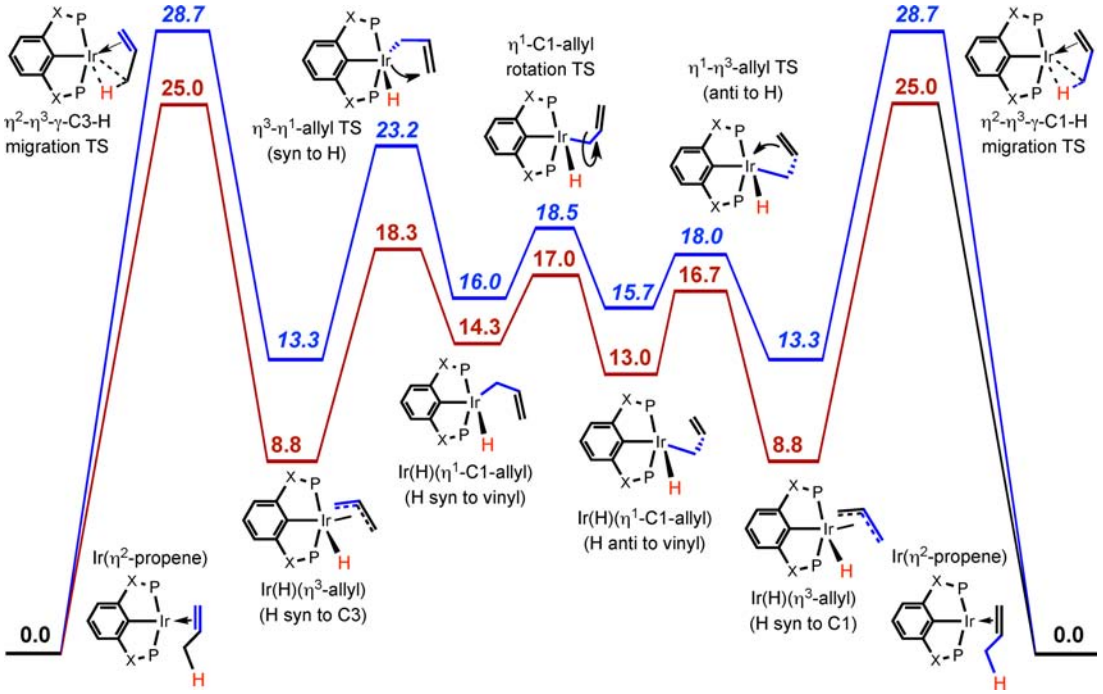

Figure 10. An η^2-η^3-η^1 rotation pathway (γ-H migration) calculated for 1,3-H migration of bound propene, ($^{t\text{Bu}}$POCOP)Ir (X = O; blue, italicized free energy values) and ($^{t\text{Bu}}$PCP)Ir (X = CH_2; red).

shown in Figure 10.[44−46] (Processes involving η^3-η^1-η^3 opening/closing have also been proposed previously to account for *syn*/*anti* exchange of allyl ligands; these processes are related to but distinct from the present pathway.[47,48]) The free energy barriers (25 °C) calculated for such an η^2-η^3-η^1 pathway for 1,3-H migration for propene are 28.7 and 25.0 kcal/mol for ($^{t\text{Bu}}$POCOP)Ir and ($^{t\text{Bu}}$PCP)Ir, respectively (Figure 10 and Table 3). At 60 °C, the value for ($^{t\text{Bu}}$POCOP)Ir is 29.0 kcal/mol, which compares adequately with the barrier determined experimentally for 1,3-deuterium migration in ($^{t\text{Bu}}$POCOP)Ir-(CD_3CHCH_2) at 60 °C, ca. 26.7 kcal/mol.

For the isomerization of (pincer)Ir(*trans*-2-hexene) to (pincer)Ir(1-hexene), the experimental value obtained for ($^{t\text{Bu}}$POCOP)Ir(*trans*-2-hexene) is 26.8 kcal/mol at 60 °C (26.5 kcal/mol when extrapolated to 25 °C) and 23.6 kcal/mol for ($^{t\text{Bu}}$PCP)Ir(*trans*-2-hexene) at 25 °C. The calculated values for this pathway, 28.0 and 24.6 kcal/mol for ($^{t\text{Bu}}$POCOP)Ir and ($^{t\text{Bu}}$PCP)Ir, respectively, are in very good agreement with experimental values.

Alternative Pathway for Allyl Formation: A σ-Complex Undergoing C−H Addition. The intermediacy of the η^1-allyl species in the η^2-η^3-η^1 pathway suggested an alternative process that might avoid the relatively high-barrier η^2-η^3 step, namely, C−H addition of a non-π-bound olefin leading *directly* to the η^1 species. Such a pathway is shown in Figure 11 for ($^{t\text{Bu}}$POCOP)Ir(η^2-propene) and ($^{t\text{Bu}}$PCP)Ir(η^2-propene). Addition of the allylic C−H bond is achieved via a slippage from π-coordination to a σ-complex of the allylic C−H bond, followed by C−H bond oxidative addition. The η^1-allyl hydride can then close to an η^3 configuration via coordination of the double bond at the position *anti* to the hydride ligand. The η^3-η^1 opening at the position *syn* to the hydride then affords an η^1-allyl hydride in which the carbon atom that initially was C1 (vinylic) now becomes an sp^3 carbon bound to iridium. C−H elimination gives a σ-complex, which slips back to an η^2-propene complex that is equivalent to the starting complex, with the coordinated propene having undergone double-bond migration. The overall barriers calculated for this pathway, 23.5 and 21.3 kcal/mol for ($^{t\text{Bu}}$POCOP)Ir and ($^{t\text{Bu}}$PCP)Ir, respectively (Figure 11), are significantly lower (by 5.2 and 3.7 kcal/mol, Table 5) than those for the η^2-η^3-η^1 rotation pathway. Extrapolated to 60 °C, the barrier is 23.7 kcal/mol for the 1,3-H

Table 3. Path of η^2-η^3-η^1 (γ-H Migration of η^2-Coordinated Alkene) for Double-Bond Migration[a]

pincer ligand	POCOP			PCP		
alkene	propene	hexene	MP-ene	propene	hexene	MP-ene
Ir + 1-alkene	14.9	15.2	15.3	4.8	5.3	5.2
Ir(η^2-1-alkene)	0.0	0.0	0.0	0.0	0.0	0.0
η^2-η^3 γ-C3−H migration TS	**28.7**	**28.0**	**28.5**	**25.0**	**27.2**	**26.9**
Ir(H)(η^3-allyl) (H *syn* to C3)	13.3	13.7	17.0	8.8	11.0	9.9
η^3-η^1-allyl TS (*syn* to H)	23.2	20.2	22.7	18.3	16.2	17.3
Ir(H)(η^1-C1-allyl) (H *syn* to vinyl)	16.0	13.3	13.1	14.3	11.7	11.5
η^1-C1-allyl rotation TS	18.5	16.0	18.9	17.0	14.5	15.5
Ir(H)(η^1-C1-allyl) (H *anti* to vinyl)	15.7	12.9	12.8	13.0	10.8	10.8
η^1-η^3-allyl TS (*anti* to H)	18.0	17.2	17.7	16.7	17.5	18.2
Ir(H)(η^3-allyl) (H *syn* to C1)	13.3	16.0	17.4	8.8	9.6	9.6
η^3-η^2-γ-C1-H migration TS	**28.7**	**29.9**	**33.0**	**25.0**	**29.0**	**30.7**
Ir(η^2-propene or 2-alkene)	0.0	1.9	6.1	0.0	4.4	7.4

[a]Free energies (kcal/mol, 25 °C) for ($^{t\text{Bu}}$POCOP)Ir and ($^{t\text{Bu}}$PCP)Ir complexes of propene, 1-hexene/2-hexene, and MP-1-ene/MP-2-ene (highest calculated TS free energies for formation of η^3-allyl complex, from each isomer, in bold font).

dx.doi.org/10.1021/ja301464c | J. Am. Chem. Soc. 2012, 134, 13276−13295

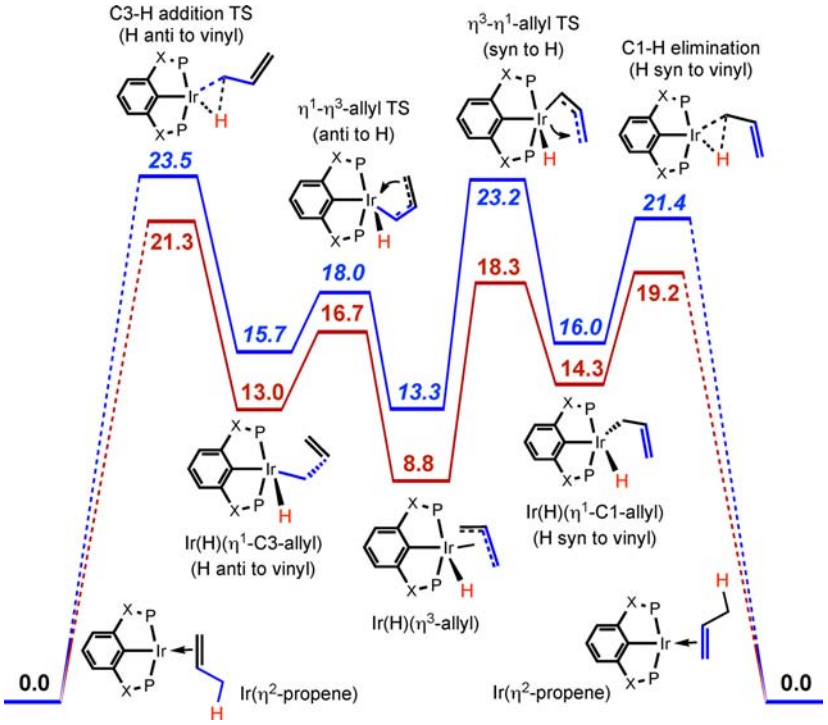

Figure 11. An η^2-η^1-η^3 pathway (C−H addition) calculated for 1,3-H migration of bound propene. ($^{t\text{Bu}}$POCOP)Ir (X = O; blue, italicized free energy values) and ($^{t\text{Bu}}$PCP)Ir (X = CH_2; red). See Supporting Information for pathway connecting the C−H addition transition states with the propene complex.

shift in ($^{t\text{Bu}}$POCOP)Ir(η^2-propene) via the η^2-η^1-η^3 C−H addition pathway, in reasonable agreement with the value of ca. 26.7 kcal/mol obtained experimentally for the 1,3-D shift.

Free energy values for the intermediates and TSs for the η^2-η^1-η^3 pathway shown in Figure 11, as well as the hexene and methylpentene analogues, are given in Table 4. A summary of experimentally obtained free energies of activation and the calculated overall free energy barriers (calculated at 25 °C and experimental temperatures for comparison purposes) is presented in Table 5. Molecular structures of the ($^{t\text{Bu}}$POCOP)-Ir intermediates and transition states are shown in Figures 12 and 13 (($^{t\text{Bu}}$POCOP)Ir was chosen for visual simplicity because the configuration of the pincer framework is much closer to planar than that of ($^{t\text{Bu}}$PCP)Ir).

Since both η^2-η^3 and η^2-η^1-η^3 pathways involve cleavage of the olefin C(3)−H bond (formally as a β-H elimination in the former case, as an oxidative addition in the latter), it may seem surprising that the lower energy TS is the one in which the double bond is not coordinated to iridium. However, there is extensive precedent for addition to d^8 species in which the TS for addition to a three-coordinate intermediate is lower in energy than the TS for addition to the corresponding four-coordinate species, despite the penalty of one less metal−ligand bond.[49] The archetypal example is Wilkinson's catalyst, $Rh(PPh_3)_3Cl$, which loses one PPh_3 ligand before it adds H_2 and then recoordinates the PPh_3.[50] Likewise, the microscopic reverse reaction, reductive elimination from six-coordinate d^6 complexes, typically proceeds via prior ligand loss.[51] More directly related to the present system, we have shown that addition of aryl C−H bonds *ortho* to coordinating groups (e.g., acetophenone) is more favorable when the *ortho* functional group is *not* coordinated; coordination of the so-called "directing" group occurs subsequent to C−H addition.[52] If the reaction with an alkene to give an allyl hydride is viewed as the coordination of a double bond and the addition of an allylic C−H bond, the precedents above would suggest that the η^2-η^1 pathway would indeed be more favorable than η^2-η^3.

Table 4. Path of η^2-η^1-η^3 (C(sp^3)−H Addition of Non-π-coordinated Alkene) for Double-Bond Migration[a]

pincer ligand	POCOP			PCP		
alkene	propene	hexene	MP-ene	propene	hexene	MP-ene
Ir + 1-alkene	14.9	15.2	15.3	4.8	5.3	5.2
Ir(η^2-1-alkene)	0.0	0.0	0.0	0.0	0.0	0.0
Ir(2-alkene-C3−H) σ-complex	17.3	23.1	24.9	13.8	17.7	21.7
C3−H add/elim TS (H *anti* to vinyl)	**23.5**	**28.4**	**29.8**	**21.3**	**27.2**	**31.6**
Ir(H)(η^1-allyl) (H *anti* to vinyl)	15.7	21.3	24.9	13.0	20.2	22.0
η^1-η^3 allyl TS (*anti* to H)	18.0	22.7	27.5	16.7	21.9	30.1
Ir(H)(η^3-allyl)	13.3	13.7	17.0	8.8	11.0	9.9
η^3-η^1 allyl TS (*syn* to H)	**23.2**	**20.2**	**22.7**	18.3	**16.2**	**17.3**
Ir(H)(η^1-allyl) (H *syn* to vinyl)	16.0	13.3	13.1	14.3	11.7	11.5
C1−H add/elim TS (H *syn* to vinyl)	21.4	18.6	18.5	**19.2**	16.1	16.2
Ir(2-alkene-C1-H) σ-complex	17.3	14.7	14.3	13.8	10.5	10.0
Ir(η^2-propene or 2-alkene)	0.0	1.9	6.1	0.0	5.3	7.4

[a]Free energies (kcal/mol, 25 °C) for ($^{t\text{Bu}}$POCOP)Ir and ($^{t\text{Bu}}$PCP)Ir complexes of propene, 1-hexene/2-hexene, and MP-1-ene/MP-2-ene (highest calculated TS free energies for formation of η^3-allyl complex, from each isomer, in bold font).

dx.doi.org/10.1021/ja301464c | J. Am. Chem. Soc. 2012, 134, 13276−13295

Table 5. Experimental and Calculated Free Energies of Activation (kcal/mol) for the Overall Isomerizations or Double-Bond Migration (Propene) Reactions (Lowest Energy Calculated Barriers for Each Pathway in Bold Font)

	Exp T	Exp $\Delta G^{\ddagger}$	$\Delta G^{\ddagger}$ (25 °C)			$\Delta G^{\ddagger}$ (Exp T)	
			η2–η1–η3	η2–η3–η1	η2-η3-η1-η2	η2–η1–η3	η2–η3–η1
(^{tBu}POCOP)Ir(propene)	60	26.7	**23.5**	28.7		23.7	29.0
(^{tBu}PCP)Ir(propene)			**21.3**	25.0			
(^{tBu}PCP)Ir(1-hexene)	125	27.9	**27.2**	29.0	**27.2**	27.2	29.5
(^{tBu}POCOP)Ir(2-hexene)	25	26.5	26.5	28.0	**26.1**	26.5	28.0
(^{tBu}PCP)Ir(2-hexene)	25	23.6	**22.8**	24.6	**22.8**	22.8	24.6
(^{tBu}POCOP)Ir(MP-2-ene)	60	24.6	23.7	26.9	**22.4**	23.6	27.0
(^{tBu}PCP)Ir(MP-2-ene)	25	23.0	24.2	23.3	**20.9**	24.2	23.3

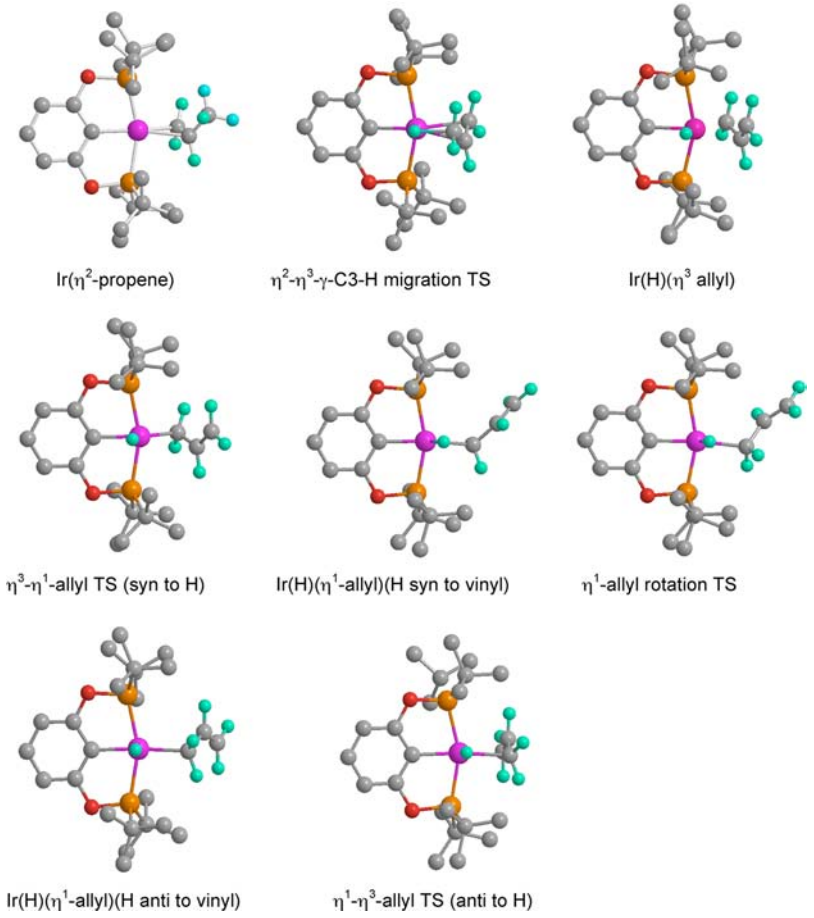

Figure 12. Molecular structures of intermediates and transition states for double-bond migration in (^{tBu}POCOP)Ir(propene) via the η^2-η^3-η^1 pathway (O = red, P = orange, Ir = purple, C = gray, selected H = blue; hydrogens on pincer ligand not shown).

The path from η^2-complex to the η^1-allylic C–H bond addition TS is not straightforward. We calculate that the olefin could fully (or nearly fully) dissociate from the metal center and return to form the σ-complex, or the olefin could "slip" to form a vinylic C–H bond σ-complex, followed by isomerization or "chain-walking" to give the allylic C–H bond σ-complex leading to oxidative cleavage.[53] For clarity, we have omitted these steps from Figure 11; the details of these calculations can be found in Supporting Information. In both cases, the calculated barriers are less than the barrier to double-bond migration, and therefore, such processes would not be rate-limiting.

Hexene Isomerization. Note that both the η^2-η^1-η^3 and η^2-η^3-η^1 pathways for propene double-bond migration are unsymmetrical as depicted in Figures 10 and 11. In particular, in either of these two pathways, the formal opening or closing of the allyl group (i.e., the η^3/η^1 transition) can first occur either *syn* or *anti* to the hydride, followed by the reverse process (closing or opening) occurring *anti* or *syn*, respectively. Thus, there are two propene 1,3-H migration pathways for each of the two mechanisms; these pathways are simply those represented by the forward and reverse direction in each figure (Figures 10 and 11). In the case of 1,2-double-bond migration of higher alkenes, however, where the η^3-allyl ligands are not symmetrical, the possibility of two distinct pathways in each direction results, one initially opening *syn* and the other initially opening *anti*. The differences in energy between these pathways, however, are not large. For the case of

dx.doi.org/10.1021/ja301464c | J. Am. Chem. Soc. 2012, 134, 13276–13295

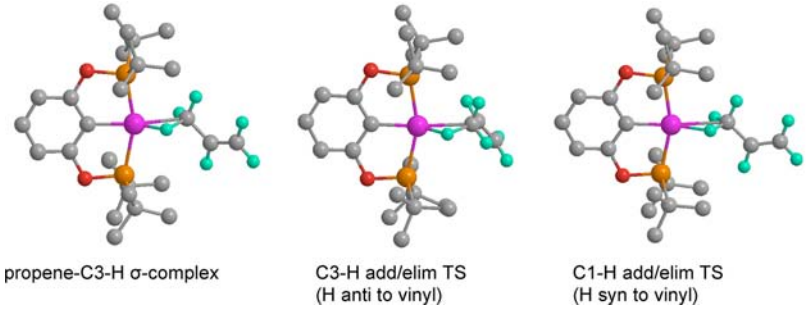

Figure 13. Molecular structures, unique to the η^2-η^1-η^3 pathway, of intermediates and transition states for double-bond migration in ($^{t\text{Bu}}$POCOP)Ir(propene) (for those species common to the η^2-η^3-η^1 pathway, see Figure 12). (O = red, P = orange, Ir = purple, C = gray, selected H atoms = blue; hydrogens on pincer ligand not shown.)

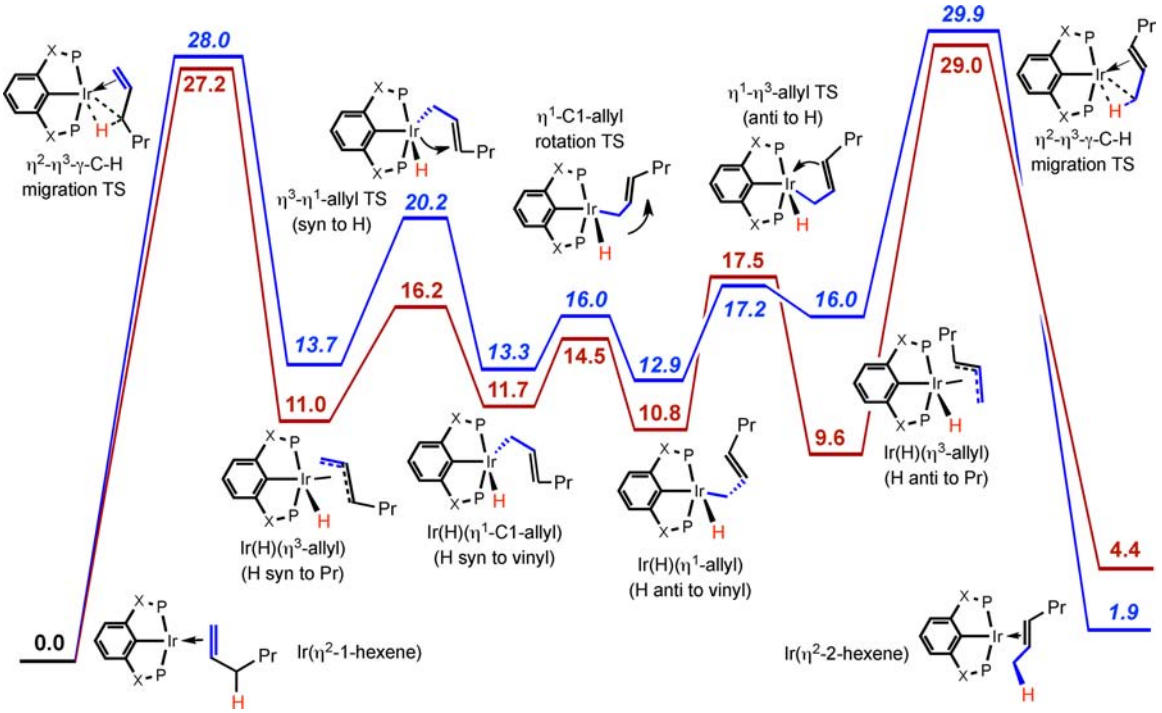

Figure 14. Pathway of η^2-η^3-η^1 (γ-H migration) calculated for isomerization of bound 1-hexene/*trans*-2-hexene, ($^{t\text{Bu}}$POCOP)Ir (X = O; blue, italicized free energy values) and ($^{t\text{Bu}}$PCP)Ir (X = CH_2; red).

interconversion of bound 1-hexene and *trans*-2-hexene, the pathway with the lower barrier is shown in Figures 14 and 15.

"Mixed" Pathways (Combined η^2-η^3-η^1 and η^2-η^1-η^3). Both η^2-η^3-η^1 and C−H addition (η^2-η^1-η^3) pathways for isomerization of 1-hexene proceed via the η^3-allyl hydride in which the *n*-Pr group bound to C3 is *syn* to the hydride (Figures 14 and 15). Proceeding from the *trans*-2-hexene adduct to that η^3-allyl hydride (right to left in Figures 14 and 15), the transition states encountered via the η^2-η^3-η^1 pathway (29.9 and 29.0 kcal/mol; Figure 14) are much higher in energy than those in the C−H addition pathway (18.6 and 16.1 kcal/mol, Figure 15). The pronounced differences in TS energies are probably well outside the error limits of the calculations. The calculated energies of the TSs for the addition/elimination of the secondary allylic C−H bond of 1-hexene, however, are fairly high (28.4 and 27.2 kcal/mol, Figure 15) and essentially equal to the values for the η^2/η^3 transition for the 1-hexene complex (28.0 and 27.2 kcal/mol, Figure 14). There is of course no intrinsic reason that the operative pathway cannot be unsymmetrical in the sense that one segment (i.e., *trans*-2-hexene to η^3-allyl) proceeds via C−H addition, while the other segment (1-hexene to η^3-allyl) proceeds via an η^2/η^3 step. Thus, the calculations very strongly support the C−H addition/elimination step for π-olefin/allyl-hydride interconversion for one segment of the pathway (i.e., the reaction or formation of the *trans*-2-hexene complex). The results are ambiguous for the reaction or formation of the 1-hexene complex, which involves addition/elimination of the secondary allylic (C3) C−H bond of 1-hexene. The overall barriers for isomerization of the *trans*-2-hexene complexes, calculated for either a symmetric pathway (C−H addition/elimination in both directions) or a "mixed" pathway (C−H addition of 2-hexene and an η^3-η^2 transition to give 1-hexene) are in good agreement with the experimental activation free energies (Table 5).

The overall barriers to isomerization of (pincer)Ir(MP-2-ene) to (pincer)Ir(MP-1-ene) proceeding via the η^2-η^3-η^1 pathway are calculated as 26.9 and 23.3 kcal/mol for $^{t\text{Bu}}$POCOP and $^{t\text{Bu}}$PCP complexes, respectively (Figure 16). The barriers for the C−H addition pathway (η^2-η^1-η^3) are 23.7 and 24.2 kcal/mol (Figure 17), not very different from the

dx.doi.org/10.1021/ja301464c | J. Am. Chem. Soc. 2012, 134, 13276−13295

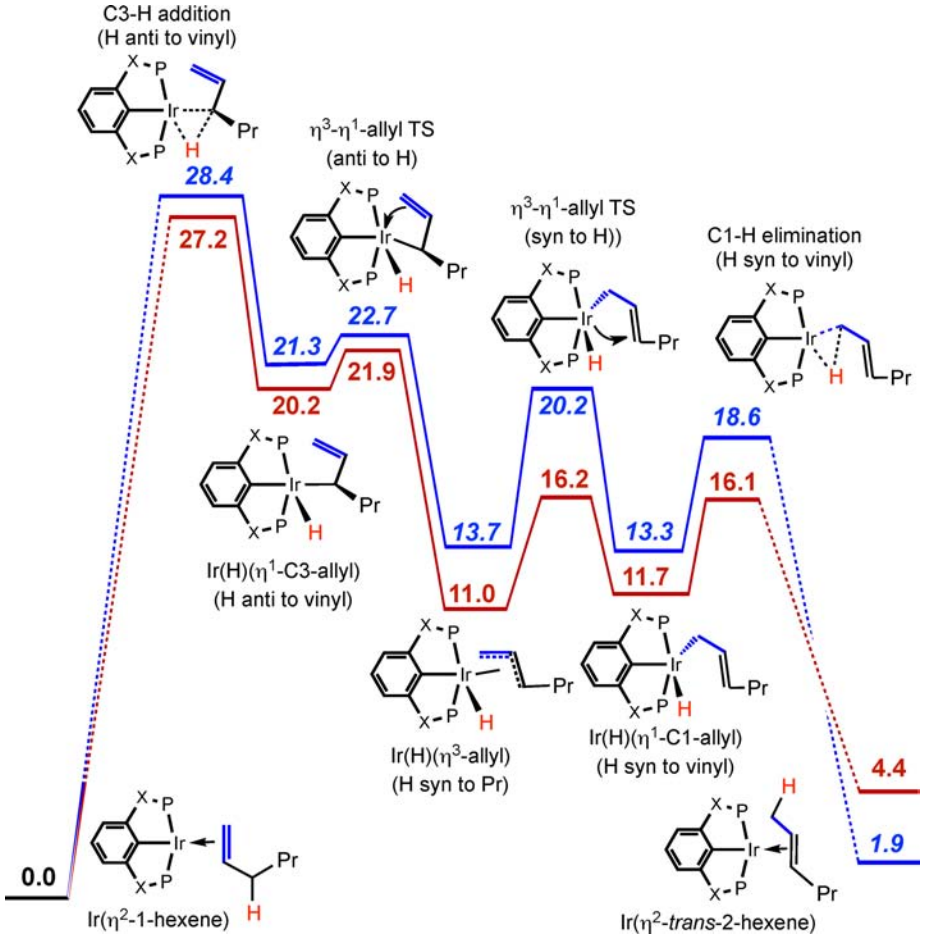

Figure 15. Pathway of η^2-η^1-η^3 (C−H addition) calculated for isomerization of bound 1-hexene/*trans*-2-hexene, ($^{t\text{Bu}}$POCOP)Ir (X = O; blue, italicized free energy values) and ($^{t\text{Bu}}$PCP)Ir (X = CH_2; red).

η^2-η^3-η^1 values, and consistent with experimental values (24.6 and 23.0 kcal/mol, respectively).

The computed values for MP-1-ene/MP-2-ene isomerization are in good agreement with experimental, but as in the case of 1-hexene/2-hexene, they only indicate a clear preference for initial C−H addition (η^2-η^1-η^3) step in one direction. For the MP-2-ene isomer, the initial C−H addition is much more favorable than the direct η^2-η^3 step. This leads to formation of the η^3-allyl with the olefin *i*-Pr group *syn* to hydride (Figures 16 and 17). Connecting the η^3-allyl with the MP-1-ene complex, however, the direct η^3/η^2 path is more favorable owing to the high energy of the very crowded secondary C−H addition/elimination TSs. Thus, the overall most favorable isomerization pathway (for both ($^{t\text{Bu}}$POCOP)Ir and ($^{t\text{Bu}}$PCP)Ir) is mixed, involving a direct C−H addition/elimination and a direct η^2/η^3 step; overall barriers via these mixed pathways are 22.4 and 20.9 kcal/mol, respectively. Note that if these values are compared with those calculated for linear hexene, the mixed pathways capture the favorable effect of branching (i.e., the observation that coordinated MP-2-ene isomerizes more rapidly than coordinated *trans*-2-hexene). In particular, the mixed pathway for ($^{t\text{Bu}}$POCOP)Ir(olefin) isomerization is calculated to be 3.7 kcal/mol lower for MP-2-ene than for *trans*-2-hexene, which is consistent with the relative rate factor of 90 obtained experimentally. In the case of ($^{t\text{Bu}}$PCP)Ir, the experimentally observed effect of branching is much smaller and indeed, the calculated difference is only 1.0 kcal/mol favoring isomerization of MP-2-ene versus 2-hexene.

Note that if only "symmetrical" pathways were considered (i.e., those proceeding via the same type of mechanism, either η^2-η^3 or η^2-η^1-η^3, for the reaction of both 1-alkene and 2-alkene species), then the isomerization of ($^{t\text{Bu}}$PCP)Ir(MP-2-ene) would actually have a PBE-calculated barrier (η^2-η^3; 23.3 kcal/mol) *greater* than that calculated for ($^{t\text{Bu}}$PCP)Ir(*trans*-2-hexene) (η^2-η^1-η^3; 21.9 kcal/mol) (Table 5), in contradiction to the experimentally observed slightly faster isomerization rate of ($^{t\text{Bu}}$PCP)Ir(MP-2-ene).

Finally, we note that M06-based calculations also support the η^2-η^1-η^3 pathway and, in fact, show an even stronger preference than do PBE-based calculations for η^2-η^1-η^3 relative to η^2-η^3 paths. Of the six cases considered in this work (double-bond migrations of propene, 1-hexene/2-hexene or MP-1-ene/MP2-ene, bound to ($^{t\text{Bu}}$PCP)Ir or ($^{t\text{Bu}}$POCOP)Ir), the M06-based calculations favor the η^2-η^1-η^3 sequence in five cases, by 6 to 8 kcal/mol versus the η^2-η^3 path. (In the case of ($^{t\text{Bu}}$PCP)Ir-(MP-2-ene) isomerization, the M06-calculated η^2-η^1-η^3 path is still more favorable, but only by 2.8 kcal/mol. Data are found in Table S23 in Supporting Information.)

■ SUMMARY AND CONCLUSION

We report that olefin isomerization catalyzed by ($^{t\text{Bu}}$PCP)Ir and ($^{t\text{Bu}}$POCOP)Ir, using the respective dihydrides as catalyst precursors, occurs by reaction of a (pincer)Ir(η^2-olefin)

dx.doi.org/10.1021/ja301464c | J. Am. Chem. Soc. 2012, 134, 13276−13295

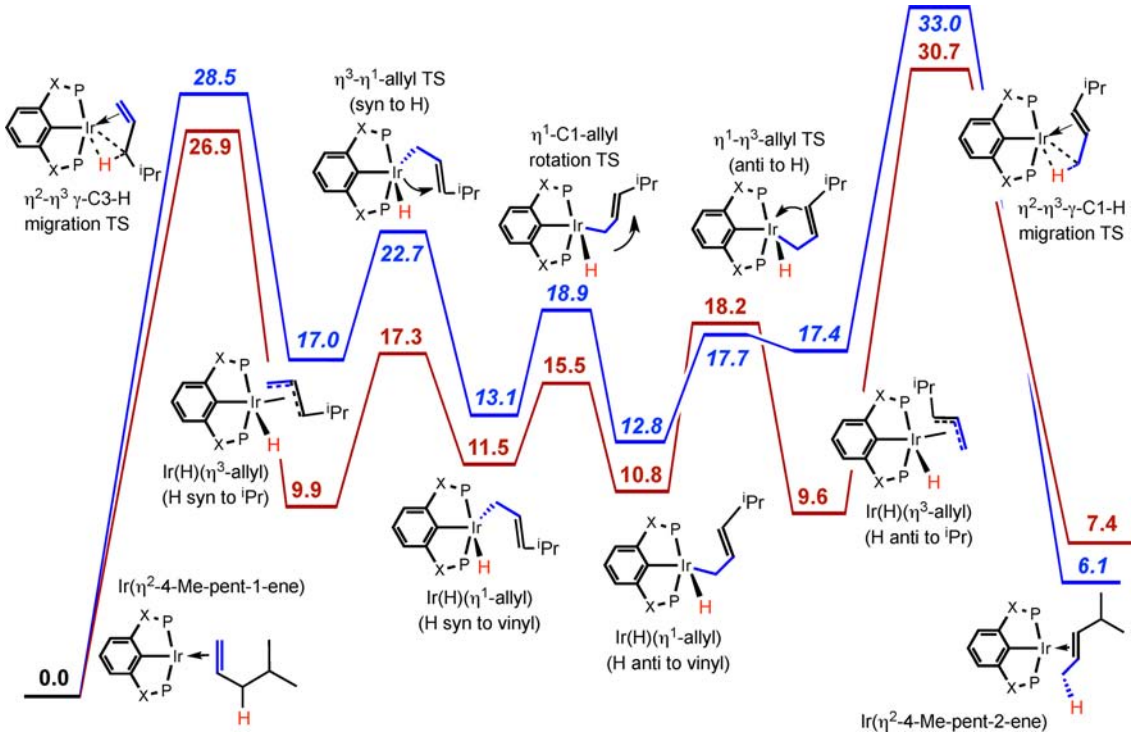

Figure 16. Calculated η^2-η^3-η^1 pathway for isomerization of bound 4-methylpent-1-ene/4-methylpent-2-ene, ($^{t\text{Bu}}$POCOP)Ir (X = O; blue, italicized free energy values) and ($^{t\text{Bu}}$PCP)Ir (X = CH_2; red).

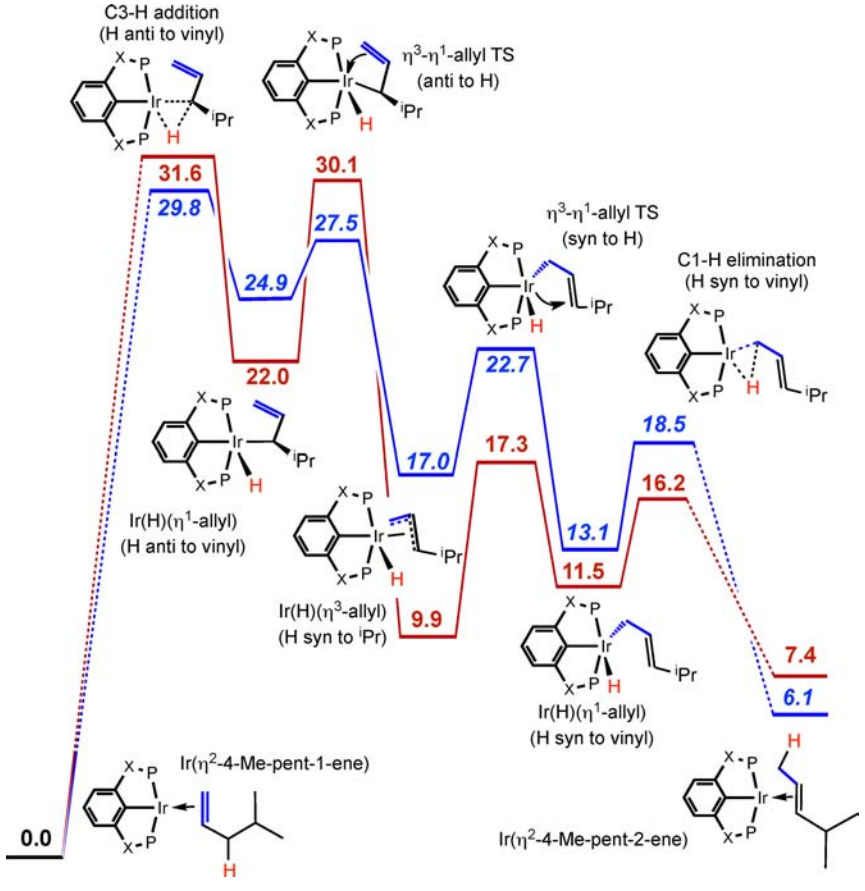

Figure 17. Calculated η^2-η^1-η^3 pathway for isomerization of bound 4-methylpent-1-ene/4-methylpent-2-ene, ($^{t\text{Bu}}$POCOP)Ir (X = O; blue, italicized free energy values) and ($^{t\text{Bu}}$PCP)Ir (X = CH_2; red).

dx.doi.org/10.1021/ja301464c | J. Am. Chem. Soc. 2012, 134, 13276−13295

complex to give a (pincer)Ir(η^3-allyl)(H) intermediate, and not via the reaction of olefin with (pincer)IrH_2. This conclusion is supported by in situ observations of the catalyst resting state, deuterium exchange experiments, and the absence of a solvent effect (alkane vs arene) on the rate of olefin isomerization. An Ir(III) η^3-allyl hydride intermediate was independently generated, characterized by low-temperature NMR spectroscopy, and shown to isomerize to the η^2-propene complex at low temperature.

Extensive computational DFT studies were conducted using two widely used combinations of functionals, PBE and M06. EXSY NMR measurements provided the rates of olefin dissociation from ($^{t\text{Bu}}$PCP)Ir(1-hexene), ($^{t\text{Bu}}$PCP)Ir(*trans*-2-hexene), ($^{t\text{Bu}}$POCOP)Ir(1-hexene), and ($^{t\text{Bu}}$POCOP)Ir(*trans*-2-hexene). The resulting values of $\Delta H^{\ddagger}$ for dissociation are all slightly higher than the PBE-derived enthalpies of binding, consistent with a small positive activation enthalpy for olefin addition to the (pincer)Ir fragments; indeed, the correlation between experimental and PBE-derived values is remarkably good. In contrast, the M06-derived binding enthalpies are significantly greater than the activation enthalpies for dissociation. Accordingly, we place greater weight on PBE-based calculations in evaluating the potential mechanisms of olefin isomerization by (pincer)Ir fragments.

The DFT calculations support the conclusion that the hydride mechanism for isomerization is not operative, as the overall barriers calculated for such a pathway are prohibitively high. An alternative mechanism in which the olefin complex reacts to give an η^3-allyl hydride, followed by in-plane rotation of the η^3-allyl ligand, and then hydride migration back to give an overall 1,3-H shift (i.e., double-bond migration) was also considered, but the barrier to in-plane η^3-allyl rotation was found to be extremely high (ca. 60 kcal/mol or greater).

A mechanism has been investigated in which the coordinated olefin undergoes (i) migration of an allylic γ-hydrogen to give an η^3-allyl hydride complex (i.e., an η^2-η^3 step), followed by (ii) η^3-η^1 allyl "opening" (*syn* or *anti* to the hydride), (iii) rotation around the Ir−C(η^1-allyl) bond, and then (iv) η^1-η^3 allyl "closing" (*anti* or *syn* to the hydride, respectively), such that the net effect of steps (ii) to (iv) is the same as an in-plane η^3-allyl rotation, and (v) the reverse of the allylic γ-hydrogen migration (i.e., an η^3-η^2 step) to give the isomerized coordinated olefin. PBE-derived barriers for such a pathway are slightly higher than experimental values, but not clearly outside the error limits of the calculations. However, PBE-based calculations yielded barriers that are lower and generally in better agreement with experiment for a "direct C−H addition" (η^2-η^1-η^3) pathway. In this latter case, formation of the η^1-allyl occurs via disruption of the Ir−olefin π-bond to give an allylic C−H σ-complex, which then undergoes oxidative cleavage. The resulting η^1-allyl undergoes η^1-η^3 allyl closing and then η^3-η^1 allyl opening in the reverse sense to effect a net 1,3-Ir shift, followed by reductive elimination to afford a C−H σ-complex, and then formation of a π-complex in which the double bond has migrated relative to the starting π-complex. Calculations using the M06 functional predicted an even stronger preference than PBE-based calculations for the "C−H addition" (η^2-η^1-η^3) pathway versus the η^2-η^3 mechanism.

Olefin isomerization has often been proposed to proceed via η^3-allyl complexes, but the mechanism of such reactions has not been well-studied.[1,2,10−14] More generally, the formation of η^3-allyl complexes from olefins is a reaction of great importance, but mechanistically, it is relatively unexplored.[54] Two aspects of the pathways described in this work are relevant in this context and, to our knowledge, have not been previously proposed: (i) dissociation of an olefin double bond from the metal center followed by C−H addition and recoordination of the double bond to give an η^3-allyl group and (ii) a net "rotation" of an η^3-allyl group via an η^3-η^1-η^3 opening−closing mechanism.

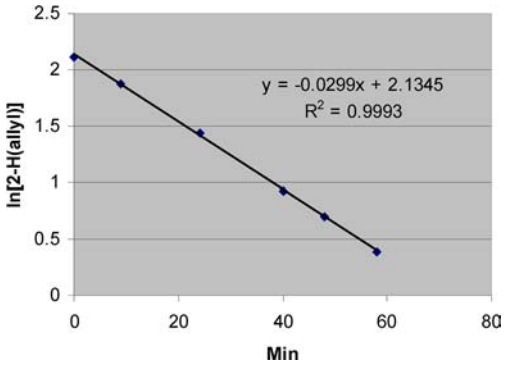

Figure 18. Plot of concentration of ln[**4**] versus time showing first-order kinetics for decay of [**4**].

EXPERIMENTAL DETAILS

General Considerations. All manipulations were carried out using standard Schlenk, high-vacuum, and glovebox techniques. Pentane and toluene were passed through columns of activated alumina. Mesitylene-d_{12} and methylcyclohexane-d_{14} were dried with 4 Å molecular sieves and degassed by freeze−pump−thaw cycles. *n*-Hexane and *tert*-butylethylene were purchased from Aldrich, dried with $LiAlH_4$ or Na/K, and transferred under vacuum into sealed flasks. Deuteride propene gases, CD_3CHCH_2, CH_3CDCH_2, and CD_3CDCD_2, were purchased from CDN and used as received. Complexes **1**[55] and **2**[37] were synthesized as previously reported.

NMR spectra were recorded on BRUKER DRX-400, AVANCE-400, and BRUKER DRX-500 MHz spectrometers. ^{1}H and ^{13}C NMR spectra were referenced to residual protio solvent peaks. ^{31}P NMR chemical shifts were referenced to an external H_3PO_4 standard.

Catalytic 1-Octene Isomerization. First, 3.0 mg of a pincer−iridium dihydride complex (5.1 mM, ($^{t\text{Bu}}$PCP)IrH_2 or ($^{t\text{Bu}}$POCOP)-IrH_2) was dissolved with 1-octene (17.0 μL, 108 mM) and mesitylene (5.0 μL, 36 mM, internal standard) in a volume of *n*-octane or *p*-xylene solvent such that the total volume of the reaction solution was 1 mL. The reaction solution was transferred into an airtight, septa-sealed vial. An initial aliquot was taken before heating the reaction to 125 °C. Reaction data were obtained via GC analysis of aliquots taken at various times during the reaction.

Isomerization of ($^{t\text{Bu}}$POCOP)Ir(2-Alkene) (*trans*-2-Hexene or *trans*-4-Methylpent-2-ene). In a J. Young tube, 6.0 mg of ($^{t\text{Bu}}$POCOP)IrH_2 (10 μmol) and 3.7 μL of the olefin (29 μmol of *trans*-2-hexene or 30 μmol of *trans*-4-methylpent-2-ene) were dissolved in 0.5 mL of *p*-xylene. All volatiles were removed in vacuo, and the solid residue was dissolved in *p*-xylene-d_{10}. No free olefins were observed in the ^{1}H NMR spectrum. The reaction solution was heated to 60 °C in the NMR spectrometer and was monitored by ^{31}P NMR spectroscopy.

Isomerization of ($^{t\text{Bu}}$PCP)Ir(*trans*-2-Hexene). In a J. Young tube, 3.0 mg of ($^{t\text{Bu}}$PCP)IrH_2 (5.1 μmol) and 32.0 μL of *tert*-butylethylene (248 μmol) were dissolved in 0.5 mL of *p*-xylene. The volume of the reaction solution was reduced in vacuo by 80%, and *p*-xylene-d_{10} was then added such that the total volume of the reaction solution was 0.5 mL. Then, 2.5 μL of *trans*-2-hexene (20 μmol) was added to the reaction solution. The reaction was monitored by ^{31}P NMR spectroscopy at 25 °C.

Isomerization of ($^{t\text{Bu}}$PCP)Ir(*trans*-4-Methylpent-2-ene). In a J. Young tube, 3.0 mg of ($^{t\text{Bu}}$PCP)IrH_2 (5.1 μmol) and 12.3 μL of *trans*-4-methylpent-2-ene (100 μmol) were dissolved in 0.5 mL of *p*-xylene-d_{10}. The reaction was monitored by ^{31}P NMR spectroscopy at 25 °C.

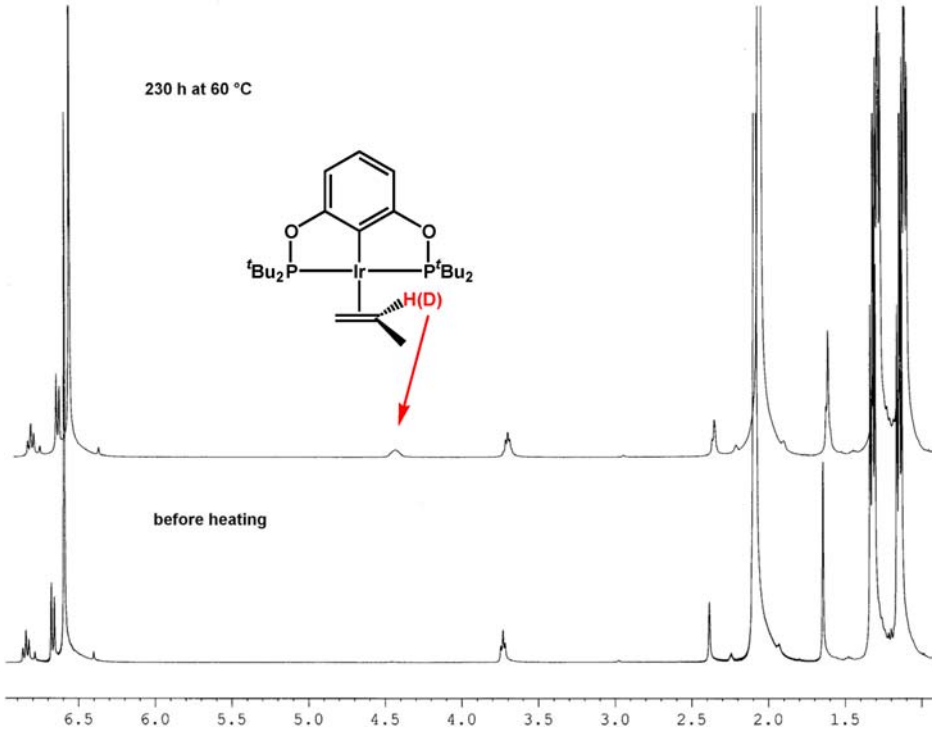

Figure 19. Overlay of ^{1}H NMR spectra showing the H/D scrambling between the central carbon and the terminal carbon of the propene ligand.

EXSY Experiments. First, 10.0 mg of a pincer−iridium dihydride complex (17 μmol) and 10.0 μL of olefin were dissolved in 0.7 mL of *p*-xylene-d_{10}. Conversion to the pincer−iridium olefin complex was complete after 30 min at 25 °C for most pincer−ligand−olefin combinations. Formation of the ($^{t\text{Bu}}$PCP)Ir(*trans*-2-hexene) complex required heating at 50 °C for 30 min to effect complete conversion to the olefin complex, and the rapid rate of olefin exchange for this complex necessitated a change in solvent to mesitylene-d_{12}. After formation of the olefin complex, a vinyl proton of the bound olefin complex was selectively irradiated in a 1D EXSY experiment, and magnetization transfer to free olefin was observed at different mixing times. The rate of olefin dissociation was determined from a plot of magnetization transfer versus mixing time.[56] These 1D EXSY experiments were performed at different temperatures, and an Eyring plot yielded activation energy parameters $\Delta H^{\ddagger}$ and $\Delta S^{\ddagger}$. Olefin exchange was confirmed to proceed via a dissociative mechanism by repeating the EXSY experiment with a much larger excess of free olefin (4- to 10-fold excess) and observing negligible change in the rate.

Synthesis of 3-d_3, 3-d_1, and 3-d_6. The respective olefins (3−5 equiv) were added to a solution of **2** (5 mg, 8.4 μmol) and toluene (0.35 mL) in a medium-walled J. Young NMR tube. After 2 h at room temperature, volatiles were evaporated under vacuum, and the resulting red solid was dried under vacuum overnight. **3-d_3**: ^{1}H NMR (162 MHz, 23 °C, Mes-d_{12}) δ 1.15 (virtual triplet, apparent J = 6.4 Hz, 18H, 2 × ^{t}Bu), 1.33 (virtual triplet, apparent J = 6.4 Hz, 18H, 2 × ^{t}Bu), 2.39 (d, $^3J_{\text{H−H}}$ = 8.0 Hz, 1H, CH_2), 3.74 (m, 1H, CH_2), 4.46 (m, 1H, CH), 6.67 (d, $^3J_{\text{H−H}}$ = 8.0 Hz, 2H), 6.84, (t, $^3J_{\text{H−H}}$ = 8.0 Hz, 1H); ^{31}P{^{1}H} NMR (400 MHz, 23 °C, Mes-d_{12}) δ 179.8 (s). **3-d_1**: ^{1}H NMR (400 MHz, 23 °C, Mes-d_{12}) δ 1.15 (virtual triplet, apparent J = 6.4 Hz, 18H, 2 × ^{t}Bu), 1.33 (virtual triplet, apparent J = 6.4 Hz, 18H, 2 × ^{t}Bu), 1.65 (s, 3H, CH_3 in propene), 2.39, (s, 1H, CH_2), 3.74 (t, $^3J_{\text{H-D}}$ = 5.6 Hz, 1H, CH_2), 6.67 (d, $^3J_{\text{H−H}}$ = 8.0 Hz, 2H), 6.84, (t, $^3J_{\text{H−H}}$ = 8.0 Hz, 1H); ^{31}P{^{1}H} NMR (162 MHz, 23 °C, Mes-d_{12}) δ 179.8 (s). **3-d_6**: ^{1}H NMR (400 MHz, 23 °C, Mes-d_{12}) δ 1.15 (virtual triplet, apparent J = 6.4 Hz, 18H, 2 × ^{t}Bu), 1.33 (virtual triplet, apparent J = 6.4 Hz, 18H, 2 × ^{t}Bu), 6.67 (d, $^3J_{\text{H−H}}$ = 8.0 Hz, 2H), 6.84, (t, $^3J_{\text{H−H}}$ = 8.0 Hz, 1H); ^{31}P{^{1}H} NMR (162 MHz, 23 °C, Mes-d_{12}) δ 179.8 (s).

Formation of the Ir(III) Hydride η^3-Allyl Complex (4). Two equivalents of allene was added to a frozen methylcyclohexane-d_{14} (0.35 mL) solution of dihydride complex **2** (9.5 mg, 16.0 μmol) in a medium-walled J. Young NMR tube. The NMR tube was shaken quickly, and when the solution was just beginning to melt, the tube was inserted into the spectrometer at −88 °C. A mixture of **4**, **2**, and propene complex **3** was observed by ^{1}H and ^{31}P NMR spectroscopy. After the complete conversion of **2** into **4** and **3**, the reaction was kept at −88 °C and monitored by NMR for 3−5 h. The mixture was then warmed to −58 °C, and the conversion of **4** to **3** was monitored by ^{1}H and ^{31}P{^{1}H} NMR spectroscopy (Figure 18): ^{1}H NMR (500 MHz, 23 °C, methylcyclohexane-d_{14}) δ −13.13 (t, 1H, $^2J_{\text{P−H}}$ = 15.0 Hz, IrH), 2.00 (br, 1H, H_{syn}), 2.13 (br, 1H, H_{syn}), 2.64 (br, 1H, H_{anti}), 2.78 (br, 1H, H_{anti}), 4.94 (br, 1H, H_2), 6.43 (d, $^3J_{\text{H−H}}$ = 7.5 Hz, 1H, H at the *meta*-position), 6.48 (d, $^3J_{\text{H−H}}$ = 7.5 Hz, 1H, H at the *meta*-position). The ^{t}Bu groups and one H at the *para*-position of the arene backbone were overlapping with those of complexes **2** and **3**: ^{31}P{^{1}H} NMR (202 MHz, 23 °C, methylcyclohexane-d_{14}) δ 152.5 (d, $J_{\text{P−P}}$ = 341 Hz), 158.5 (d, $J_{\text{P−P}}$ = 341 Hz). 13.13 (t, 1H).

Intraligand Deuterium/Hydrogen Exchange. A mesitylene-d_{12} (0.35 mL) solution of **3-d_3** or **3-d_1** (see Scheme 8) (8.4 μmol) in a medium-walled J. Young NMR tube was heated at 60 or 125 °C. Periodically, the tube was cooled to room temperature and monitored by NMR spectroscopy (Figure 19).

Ligand Exchange Reaction of 3-d_6. Two equivalents of propene was added to a mesitylene-d_{12} (0.35 mL) solution of **3-d_6** (8.4 μmol) in a medium-walled J. Young NMR tube. The tube was heated to 60 °C. Periodically, the tube was cooled to room temperature and monitored by NMR spectroscopy.

■ COMPUTATIONAL METHODS

All calculations used DFT methodologies implemented in the Gaussian 09 series of electronic structure programs.[32] Most of the data presented in the text result from calculations which employed the PBE set of functionals.[33] We did, however, also examine most pathways using the collection of functionals denoted M06.[34] For Ir, we applied the Hay−Wadt relativistic effective (small) core potential[57] and the LANL2TZ basis set[57,58] augmented by a diffuse d-type function (exponent = 0.07645); all other atoms received 6-311G(d,p) basis sets.[59,60] The results obtained with the PBE functionals were deemed overall superior to those obtained at the M06 level.

dx.doi.org/10.1021/ja301464c | J. Am. Chem. Soc. 2012, 134, 13276−13295

Standard geometry optimization procedures were followed to obtain geometries and potential energies for stationary points along the reaction paths. Normal mode analysis was performed to verify the nature of a particular stationary point (minimum or transition state). The resulting set of vibrational frequencies was employed (without scaling) to determine zero-point energy corrections. Enthalpies (ΔH, $\Delta H^{\ddagger}$) and Gibbs' free energies (ΔG, $\Delta G^{\ddagger}$; T = 298.15 K, P = 1 atm) were subsequently obtained from the potential energies (ΔE, $\Delta E^{\ddagger}$) using standard thermodynamic corrections.[61] Increased atomic grid sizes were used for numerical integrations to enhance computational stability and accuracy[62] in geometry optimizations and normal mode calculations (grid = ultrafine option).[63] Geometries of stationary points and tables containing energetic quantities are available as Supporting Information. Solvation effects were not considered explicitly in the calculations since the experiments uniformly were carried out in nonpolar hydrocarbons.

■ ASSOCIATED CONTENT

Supporting Information

Tables of relative electronic energies, enthalpies, entropies and free energies, and Cartesian coordinates and absolute energies for all minima and transition states shown in the figures. Eyring plots of EXSY kinetic data. Complete reference 32. This material is available free of charge via the Internet at http://pubs.acs.org.

■ AUTHOR INFORMATION

Corresponding Author

mbrookhart@unc.edu; kroghjes@rutgers.edu; alan.goldman@rutgers.edu

Notes

The authors declare no competing financial interest.

■ ACKNOWLEDGMENTS

We acknowledge funding by the NSF (Grant CHE-0650456) as part of the Center for Enabling New Technologies through Catalysis (CENTC).

■ REFERENCES

(1) Herrmann, W. A.; Prinz, M. In *Applied Homogeneous Catalysis with Organometallic Compounds*, 2nd ed.; Cornils, B., Herrmann, W. A., Eds.; Wiley-VCH Verlag GmbH: Weinheim, Germany, 2002; Vol. 3, p 1119−1130.

(2) Crabtree, R. H. In *The Organometallic Chemistry of the Transition Metals*, 5th ed.; John Wiley & Sons: Hoboken, NJ, 2009; pp 229−231.

(3) Mol, J. C. *J. Mol. Catal. A* **2004**, *213*, 39−45.

(4) van Leeuwen, P. W. N. M. In *Homogeneous Catalysis: Understanding the Art*; Kluwer Academic Publishers: Dordrecht, The Netherlands, 2004; pp 101−107.

(5) Schmidt, B. *Eur. J. Org. Chem.* **2004**, 1865−1880.

(6) Otsuka, S.; Tani, K. *Transition Metals for Organic Synthesis*, 2nd ed.; Wiley: New York, 2004; Vol. *1*, pp 199−209.

(7) Seayad, A.; Ahmed, M.; Klein, H.; Jackstell, R.; Gross, T.; Beller, M. *Science* **2002**, *297*, 1676−1678.

(8) Scarso, A.; Colladon, M.; Sgarbossa, P.; Santo, C.; Michelin, R. A.; Strukul, G. *Organometallics* **2010**, *29*, 1487−1497.

(9) Casey, C. P.; Cyr, C. R. *J. Am. Chem. Soc.* **1973**, *95*, 2240−2248.

(10) Manuel, T. A. *J. Org. Chem.* **1962**, *27*, 3941−3945.

(11) Alper, H.; LePort, P. C.; Wolfe, S. *J. Am. Chem. Soc.* **1969**, *91*, 7553−7554.

(12) Cowherd, F. G.; Von Rosenberg, J. L. *J. Am. Chem. Soc.* **1969**, *91*, 2157−2158.

(13) Misono, M.; Grabowski, W.; Yoneda, Y. *J. Catal.* **1977**, *49*, 363−368.

(14) Casey, C. P.; Cyr, C. R. *J. Am. Chem. Soc.* **1973**, *95*, 2248−2253.

(15) Goldman, A. S.; Roy, A. H.; Huang, Z.; Ahuja, R.; Schinski, W.; Brookhart, M. *Science* **2006**, *312*, 257−261.

(16) Bailey, B. C.; Schrock, R. R.; Kundu, S.; Goldman, A. S.; Huang, Z.; Brookhart, M. *Organometallics* **2009**, *28*, 355−360.

(17) Burnett, R. L.; Hughes, T. R. *J. Catal.* **1973**, *31*, 55−64.

(18) (a) Vidal, V.; Theolier, A.; Thivolle-Cazat, J.; Basset, J.-M. *Science* **1997**, *276*, 99. (b) Le Roux, E.; Taoufik, M.; Copéret, C.; de Mallmann, A.; Thivolle-Cazat, J.; Basset, J.-M.; Maunders, B. M.; Sunley, G. J. *Angew. Chem.* **2005**, *44*, 6755. (c) Basset, J. M.; Coperet, C.; Lefort, L.; Maunders, B. M.; Maury, O.; Le Roux, E.; Saggio, G.; Soignier, S.; Soulivong, D.; Sunley, G. J.; Taoufik, M.; Thivolle-Cazat, J. *J. Am. Chem. Soc.* **2005**, *127*, 8604. (d) Le Roux, E.; Taoufik, M.; Baudouin, A.; Coperet, C.; Thivolle-Cazat, J.; Basset, J.-M.; Maunders, B. M.; Sunley, G. J. *Adv. Synth. Catal.* **2007**, *349*, 231.

(19) (a) Dry, M. E. *Catal. Today* **2002**, *71*, 227−241. (b) Schulz, H. *Appl. Catal., A* **1999**, *186*, 3−12.

(20) (a) International Energy Agency (IAE) World Energy Outlook 2008, pp 250−261, http://www.worldenergyoutlook.org/2008.asp. (b) Ayala, L. F.; Kouassi, J. P. *Energy Fuels* **2007**, *21*, 1592.

(21) (a) Schrock, R. R. *Chem. Commun.* **2005**, 2773−2777. (b) Fox, H. H.; Lee, J. K.; Park, L. Y.; Schrock, R. R. *Organometallics* **1993**, *12*, 759−768. (c) Schrock, R. R.; Murdzek, J. S.; Bazan, G. C.; Robbins, J.; DiMare, M.; O'Regan, M. *J. Am. Chem. Soc.* **1990**, *112*, 3875−3886.

(22) Liu, F.; Pak, E. B.; Singh, B.; Jensen, C. M.; Goldman, A. S. *J. Am. Chem. Soc.* **1999**, *121*, 4086−4087.

(23) Choi, J.; MacArthur, A. H. R.; Brookhart, M.; Goldman, A. S. *Chem. Rev.* **2011**, *111*, 1761−1779.

(24) Krogh-Jespersen, K.; Czerw, M.; Summa, N.; Renkema, K. B.; Achord, P. D.; Goldman, A. S. *J. Am. Chem. Soc.* **2002**, *124*, 11404−11416.

(25) Göttker-Schnetmann, I.; Brookhart, M. *J. Am. Chem. Soc.* **2004**, *126*, 9330−9338.

(26) Biswas, S.; Brookhart, M.; Goldman, A. S.; Krogh-Jespersen, K. Manuscript in preparation.

(27) (a) McGhee, W. D.; Bergman, R. G. *J. Am. Chem. Soc.* **1985**, *107*, 3388. (b) McGhee, W. D.; Bergman, R. G. *J. Am. Chem. Soc.* **1988**, *110*, 4246.

(28) Tulip, T. H.; Ibers, J. A. *J. Am. Chem. Soc.* **1979**, *101*, 4201−4211.

(29) Wakefield, J. B.; Stryker, J. M. *J. Am. Chem. Soc.* **1991**, *113*, 7057.

(30) NIST Chemistry WebBook; NIST Standard Reference Database Number 69. http://webbook.nist.gov/chemistry/.

(31) Hoops, S.; Sahle, S.; Gauges, R.; Lee, C.; Pahle, J.; Simus, N.; Singhal, M.; Xu, L.; Mendes, P.; Kummer, U. *Bioinformatics* **2006**, *22*, 3067−3074.

(32) Frisch, M. J.; et al., *Gaussian 09*, revision A.02; Gaussian, Inc.: Wallingford, CT, 2009. See Supporting Information for the complete reference to Gaussian 09.

(33) Perdew, J. P.; Burke, K.; Ernzerhof, M. *Phys. Rev. Lett.* **1996**, *77*, 3865.

(34) Zhao, C. Y.; Truhlar, D. G. *Theo. Chem. Acc.* **2008**, *120*, 215−241.

(35) Göttker-Schnetmann, I.; White, P.; Brookhart, M. *J. Am. Chem. Soc.* **2004**, *126*, 1804−1811.

(36) Punji, B.; Emge, T. J.; Goldman, A. S. *Organometallics* **2010**, *29*, 2702−2709.

(37) Göttker-Schnetmann, I.; White, P. S.; Brookhart, M. *Organometallics* **2004**, *23*, 1766−1776.

(38) Lee, D. W.; Kaska, W. C.; Jensen, C. M. *Organometallics* **1998**, *17*, 1−3.

(39) Bondi, A. *J. Phys. Chem.* **1964**, *68*, 441−451.

(40) Pauling, L. *The Nature of the Chemical Bond*, 3rd ed.; Cornell University Press: Ithaca, NY, 1960.

(41) Zhu, K.; Achord, P. D.; Zhang, X.; Krogh-Jespersen, K.; Goldman, A. S. *J. Am. Chem. Soc.* **2004**, *126*, 13044−13053.

(42) Becconsall, J. K.; O'Brien, S. *Chem. Commun.* **1966**, 720−722.

(43) Faller, J. W.; Incorvia, M. J. *Inorg. Chem.* **1968**, *7*, 840−842.

(44) Fish, R. W.; Giering, W. P.; Marten, D.; Rosenblum, M. *J. Organomet. Chem.* **1976**, *105*, 101−118.

(45) Gibson, D. H.; Hsu, W.-L.; Steinmetz, A. L.; Johnson, B. V. *J. Organomet. Chem.* **1981**, *208*, 89−102.
(46) Ariafard, A.; Bi, S. W.; Lin, Z. Y. *Organometallics* **2005**, *24*, 2241−2244.
(47) Sprinz, J.; Kiefer, M.; Helmchen, G.; Reggelin, M.; Huttner, G.; Walter, O.; Zsolnai, L. *Tetrahedron Lett.* **1994**, *35*, 1523−1526.
(48) Trost, B. M.; Van, V. D. L. *Chem. Rev.* **1996**, *96*, 395−422.
(49) The classic explanation for the high barrier to addition of H−H or C−H bonds to four-coordinate d^8 metal centers (or elimination from six-coordinate d^6 centers) was proposed by Hoffmann: Saillard, J.; Hoffmann, R. *J. Am. Chem. Soc.* **1984**, *106*, 2006−2026. For a more recent lead reference concerning this issue, see: Crumpton-Bregel, D. M.; Goldberg, K. I. *J. Am. Chem. Soc.* **2003**, *125*, 9442−9456.
(50) Halpern, J.; Wong, C. S. *J. Chem. Soc., Chem. Commun.* **1973**, 629−630.
(51) Bartlett, K. L.; Goldberg, K. I.; Borden, W. T. *J. Am. Chem. Soc.* **2000**, *122*, 1456−1465.
(52) Zhang, X.; Kanzelberger, M.; Emge, T. J.; Goldman, A. S. *J. Am. Chem. Soc.* **2004**, *126*, 13192−13193.
(53) Vetter, A. J.; Flaschenriem, C.; Jones, W. D. *J. Am. Chem. Soc.* **2005**, *127*, 12315−12322.
(54) Jensen, T.; Fristrup, P. *Chem.—Eur. J.* **2009**, *15*, 9632−9636.
(55) Gupta, M.; Hagen, C.; Flesher, R. J.; Kaska, W. C.; Jensen, C. M. *Chem. Commun.* **1996**, 2083−2084.
(56) Perrin, C. L.; Dwyer, T. J. *Chem. Rev.* **1990**, *90*, 935−967.
(57) Hay, P. J.; Wadt, W. R. *J. Chem. Phys.* **1985**, *82*, 299.
(58) Roy, L. E.; Hay, P. J.; Martin, R. L. *J. Chem. Theory Comput.* **2008**, *4*, 1029−1031.
(59) Krishnan, R.; Binkley, J. S.; Seeger, R.; Pople, J. A. *J. Chem. Phys.* **1980**, *72*, 650−654.
(60) McLean, A. D.; Chandler, G. S. *J. Chem. Phys.* **1980**, *72*, 5639−5648.
(61) McQuarrie, D. A. *Statistical Thermodynamics*; Harper and Row: New York, 1973.
(62) Wheeler, S. E.; Houk, K. N. *J. Chem. Theory Comput.* **2010**, *6*, 395−404.
(63) Frisch, Æ.; Frisch, M. J.; Clemente, F. R.; Trucks, G. W. *Gaussian 09 User's Reference*, 147.

■ NOTE ADDED IN PROOF

We recently became aware of a report by Green and Hughes in 1976, in which it was proposed that the isomerization of an iron-coordinated olefin proceeded via an η^1-allyl complex that was *not* formed via an η^3-allyl intermediate. The evidence for this proposal was based on elegant stereochemical studies and is complementary to the computational support for the η^1-allyl mechanism proposed in this work. See: Green, M.; Hughes, R. P. *J. Chem. Soc., Dalton Trans.* **1976**, 1907.